Virtual Statistical Energy Analysis Applied to Naval NVH Models

submitted on 19 June 2020

by

ANDRADE PAIVA André Antonio | Vieux Chemin de Namur 24 | 1340 Ottignies-Louvain-la-Neuve |
andre.andrade.paiva@gmail.com

Student ID No.: 219 200 148

Master Thesis

This page is intentionally left blank

Declaration of Authorship

I declare that this thesis and the work presented in it are my own and have been generated by me as the result of my own original research.

Where I have consulted the published work of others, this is always clearly attributed.

Where I have quoted from the work of others, the source is always given. With the exception of such quotations, this thesis is entirely my own work.

I have acknowledged all main sources of help.

Where the thesis is based on work done by myself jointly with others, I have made clear exactly what was done by others and what I have contributed myself.

This thesis contains no material that has been submitted previously, in whole or in part, for the award of any other academic degree or diploma.

I cede copyright of the thesis in favour of the University of Rostock

Date: 18/06/2020   Signature:

This page is intentionally left blank

ABSTRACT

As the noise standards and regulations become more demanding, the evaluation of vibroacoustic problems is frequently incorporated in the design cycle of the modern means of transportation. Typically, these problems occur at high-frequency ranges where the analysis becomes more complex due to the modal overlap and increased density of the resonant modes.

Differently from a deterministic approach that evaluates specific local magnitudes of a model, methods such as the Statistical Energy Analysis (SEA) were developed to evaluate the global behavior of a model based on the energetic values as a variable. In the SEA approach, a model is divided into subsystems and an energy transfer matrix is determined. Typically, this matrix is referred to as the SEA matrix and it will describe the energy flow of the model for any given linear excitation. Besides, these energies will allow the evaluation of the averaged sound pressure, stresses, and strains of each subsystem.

In the context of finite element models, the mass and stiffness matrices are projected over the modal basis which defines the distribution of these properties according to the resonant modes. These matrices are referred to as distribution matrices. Such matrices provide an efficient way to evaluate the energetic behavior of the finite element model, which in turn enables to set up a virtualization of the experimental methods giving access to the SEA matrix (such as the Power Injection Method). Nevertheless, the numerical approach requires the modal extraction and the assembly of the distribution matrices, which for most of the practical cases of interest will contain hundreds of thousands of modes, increasing the analysis computational cost. In the context of optimization, which requires testing different design configurations, these costly procedures have to be re-performed for each iteration, which often leads to an unfeasible computational effort. Therefore, the main objective of this study is to provide a method that allows the change of the mass, stiffness, and damping of each subsystem without re-performing the modal extraction of the model and building its distribution matrices.

Throughout the study, distinct approximation procedures were implemented, with an increasing complexity in order to obtain more accurate approximations. It will be demonstrated that this iterative process converged to an efficient method to predict the changes in the energetic model for a negligible cost. An optimization tool will be demonstrated on a model and its results compared with a reference model with the re-computed modal basis. The whole scope of this master thesis has been implemented within the source code of the commercial software Actran developed by the company Free Field Technologies, part of Hexagon.

This page is intentionally left blank

CONTENT

LIST OF FIGURES

LIST OF TABLES

This page is intentionally left blank

1. INTRODUCTION

In this section, vibroacoustic analysis in high-frequency ranges will be introduced along with the main motivations for this type of analysis from an industrial perspective. It is shown how numerical methods can deal with such problems and the main difficulties of numerical analysis at a high-frequency range. Based on the given background, the objective proposed by this thesis will also be explained.

1.1 Vibroacoustics Analysis

As governmental regulations become stricter to diminish the harm and noise pollution caused by the means of transportation, added to an ever-growing demanding market, the design cycles of new projects are to be shortened, and often optimization procedures are performed to achieve an optimal configuration. For each product, distinct criteria must be evaluated, for example, vessels such as cruise ships, yachts, and even ferries will require a low noise level in the passenger's cabin and common areas to guarantee their comfort during the journey, while tankers and container ships will have to comply to strict rules preventing high noise level in regions such as the engine room and crew cabins since it is important to control the exposure to excessive noise to increase the work efficiency and protect the personal healthcare.

Reliable numerical tools are required to predict and avoid excessive noise and vibration levels, especially at early design phases. If the behavior of a complex structure such as ships, airplanes, automotive vehicles, etc is accurately predicted, then strategies can be adapted to efficiently utilize resources, instead of relying on the addition of damping material all over the design's structure. This can lead to weight reduction and environmental benefits since usually, damping materials are non-recyclable. It is also evident that any vibroacoustic irregularity must be identified and dealt with as early as possible since solutions are likely to affect other engineering fields.

Traditionally, a deterministic approach, allied with the finite element method, is used to tackle down vibroacoustic problems. This provides reliable results for lower frequency ranges. However, as the noise levels of design become more relevant, higher frequency ranges must be considered. As stated in De Langue (1996) [1], a common definition of a high-frequency range is when the wavelength becomes small when comparing with structure dimensions.

In the low-frequency ranges, the modes are spaced and distinct. When the frequency is increased, the number of modes increases, and some of these modes start to overlap.

In a deterministic approach, the equation of motion is utilized to solve forced response problems, such as

$$M\frac{d^2U(t)}{dt^2} + KU(t) = F(t) \tag{1.1}$$

where $U(t)$ is the generalized displacement, M is the mass, K is the stiffness and $F(t)$ is a time-harmonic force.

For a steady-state solution, the response can be computed as

$$U = [K - \omega^2 M]^{-1} F \tag{1.2}$$

where ω^2 is the eigenfrequency.

Therefore, as seen in the Eq. 1.2, the modes will affect directly the response. As the frequency increases, there is not a clear distinction between the modes and the method becomes less accurate.

To illustrate this behavior, a direct response analysis has been done with Actran on a representation of an aluminum plate with a finite element mesh of size 1 millimeter. A unitary harmonic force is applied at the location x = 0.2 m and y = 0.1 m, the edges of the plate are simply supported, and the mean squared velocities are evaluated. The plate model and its boundaries conditions are illustrated in Figure 1 and its mechanical properties in Table 1
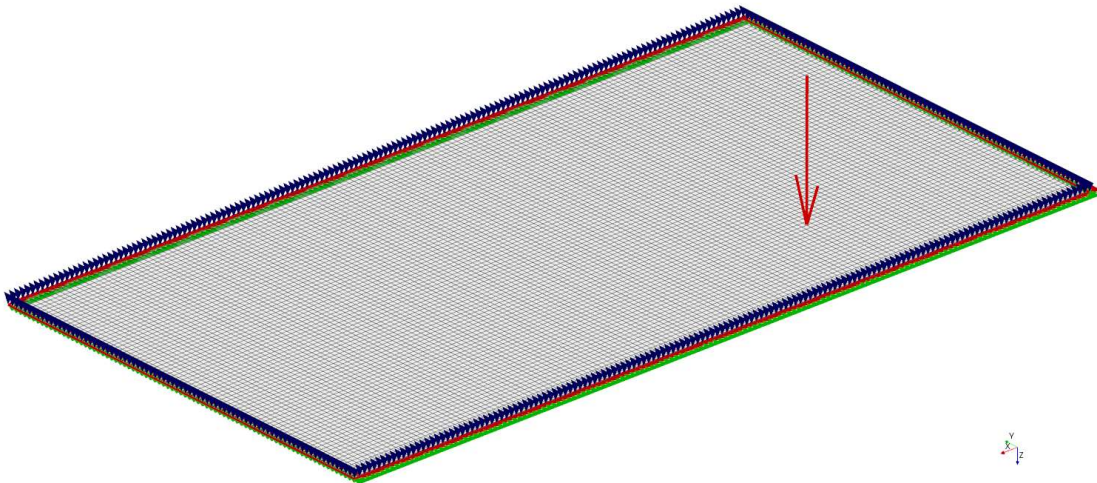
Figure 1. Finite element representation of an aluminum plate with its boundary conditions

Table 1. Mechanical properties and dimension of the aluminum plate

Plate properties		Units
Length	0.75	m
Width	0.4	m
Thickness	0.003	m
Young's Modulus	7.00E+10	Pa
Poisson coefficient	0.25	-
Mass density	2400	kg/m^3

The displacement amplitude in the z-direction of a point located at x = 0.2 m and y = 0.1 m are measured and plotted in Figure 2. It is seen that for a low-frequency range, between 0 Hz and 250 Hz, the amplitudes are spaced and distinct. However, starting from 250 Hz, modal overlapping occurs.
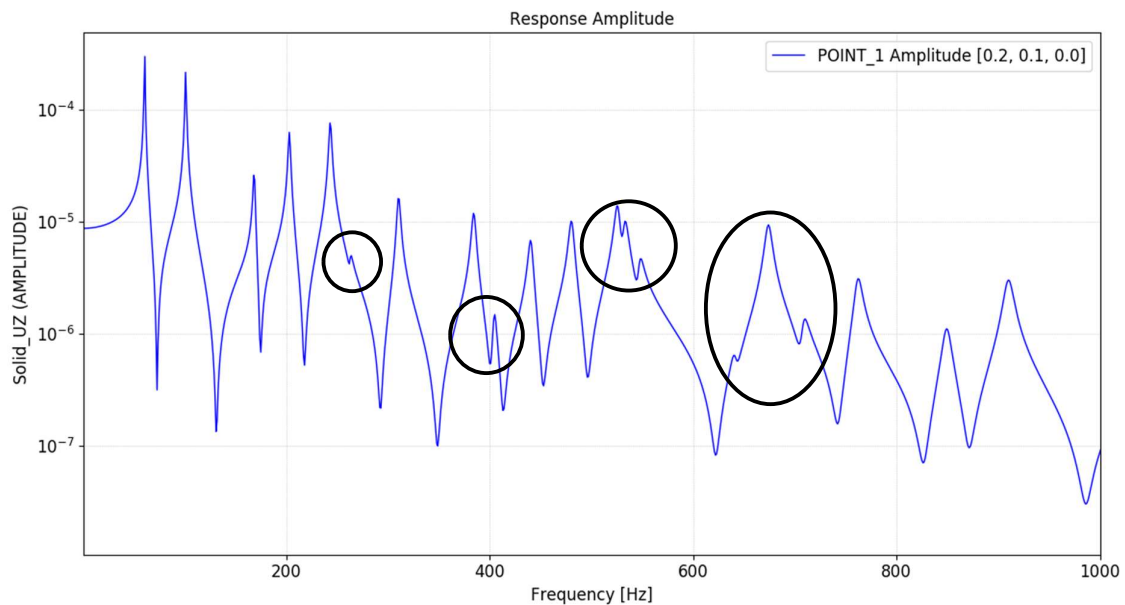
Figure 2. Amplitude response in z-direction from 1 to 1000 Hz

As the frequencies increase, in Figure 3 the modal overlap is frequent and modal densities are high. Therefore, to increase the precision from a deterministic perspective, the mesh must be refined which will implicate an additional computational cost, and still, the solution might not be as accurate as desired.
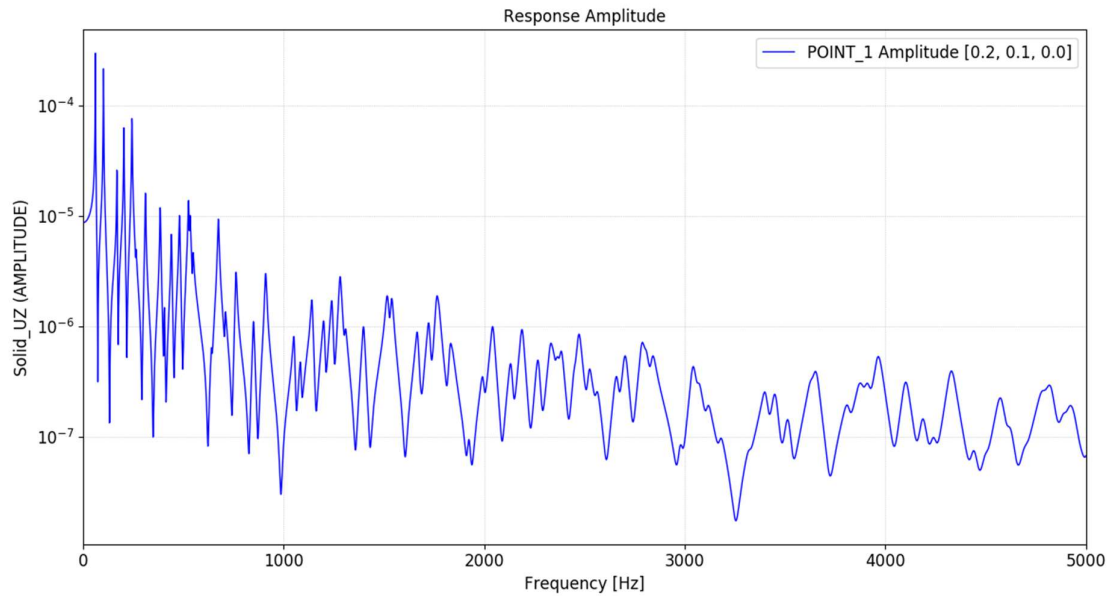
Figure 3. Amplitude response in z-direction from 1 to 5000 Hz

The impact of the high frequency on the method's accuracy can be shown by increasing the plate stiffness by 1%. With this modification, the model becomes stiffer but with a low change magnitude. It is seen in Figure 4 that indeed the changes are very slight in the lower frequencies. However, as the frequency increase, the changes become more significant. This can be related to the poor accuracy of the method for high-frequency ranges since, for such a small change, the perturbation of the results should be linear over the frequency range.
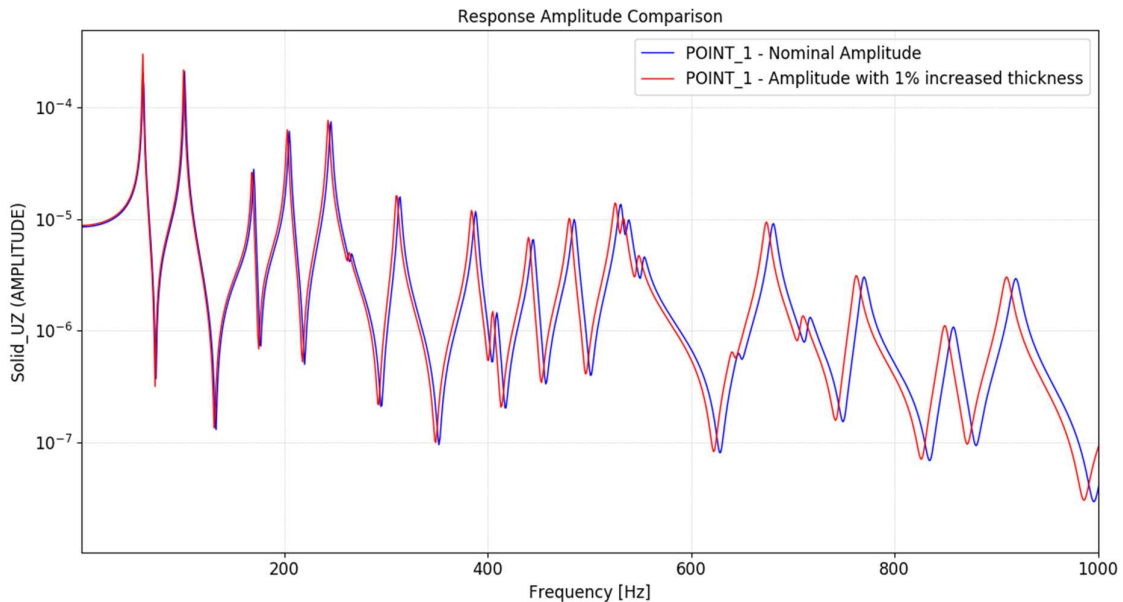
Figure 4. Amplitude response comparison in z-direction from 1 to 1000 Hz

1.2 Noise Propagation from and in Ships

When it comes to noise propagation in ships, there are several aspects to be considered, since, within a design, there are different machines and structural aspects that will determine the global vibroacoustic behavior of the structure. It is possible to identify two main propagations of interest: the noise transmitted within the ship and the noise transmitted to the environment. The first will mostly have an impact on the comfort of the passengers, communication, and health preservation of employees. The latter will impact the marine life and the population that lives near port areas.

The main classification societies under the International Association of Classification Societies (IACS) determine specifications related to onboard noise control, often based on the IMO (International Maritime Organization) resolution MSC.337(91) code on noise levels on board ships. In this statutory document [2], noise levels are segregated by work, navigation, accommodation, services, and normally unoccupied spaces. Table *2* illustrates the acceptable sound pressure in dB(A) according to the gross tonnage of the ship.

Table 2. Noise level limits for various spaces. Available from http://www.imo.org/en/KnowledgeCentre/IndexofIMOResolutions/Maritime-Safety-Committee-(MSC)/Documents/MSC.337(91).pdf [Accessed 30 May 2020]

Designation of rooms and spaces	Ship size	
	1,600 up to 10,000 GT	≥10,000 GT
4.2.1 Work spaces (see 5.1)		
Machinery spaces	110	110
Machinery control rooms	75	75
Workshops other than those forming part of machinery spaces	85	85
Non–specified work spaces (other work areas)	85	85
4.2.2 Navigation spaces		
Navigating bridge and chartrooms	65	65
Look-out posts, incl. navigating bridge wings and windows	70	70
Radio rooms (with radio equipment operating but not producing audio signals)	60	60
Radar rooms	65	65
4.2.3 Accommodation spaces		
Cabin and hospitals	60	55
Messrooms	65	60
Recreation rooms	65	60
Open recreation areas (external recreation areas)	75	75
Offices	65	60
4.2.4 Service spaces		
Galleys, without food processing equipment operating	75	75
Serveries and pantries	75	75
4.2.5 Normally unoccupied spaces		
Spaces referred to in section 3.14	90	90

In working areas that are not specified above and where the tolerated sound pressure is higher, there are rules concerning the required hearing protection equipment and the time of exposure, as shown in Figure 5.
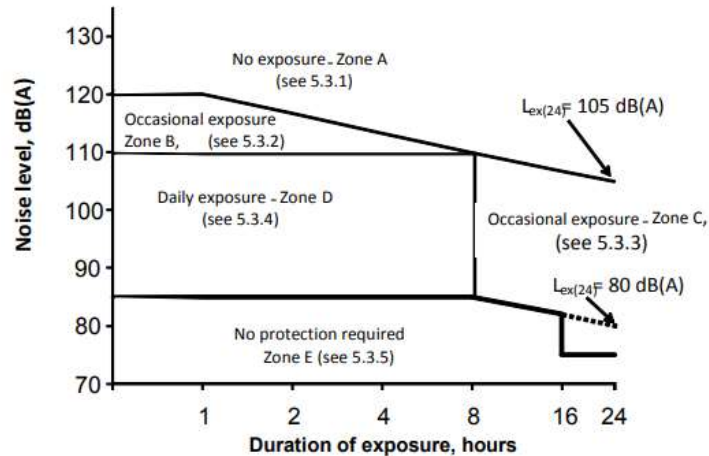
Figure 5. Noise level allowance for daily and occasionally occupational zones. Available from http://www.imo.org/en/KnowledgeCentre/IndexofIMOResolutions/Maritime-Safety-Committee-(MSC)/Documents/MSC.337(91).pdf [Accessed 30 May 2020]

Regarding the underwater noise transmitted to the environment, there is no compulsory regulation to be complied with. However, due to increasing concern about environment preservation, the IMO and many of the classification societies have developed guidelines to orientate the underwater noise measurement and reduction strategies. In addition, some classification societies have additional class notations about the underwater radiated noise, with additional certificates for the compliant designs. Thus, this is a topic that is expected to be recurrent in the following years, since more awareness and studies are being performed to evaluate the impact of ships in the marine environment.

As stated by Southall et al. (2017) [3], the hearing range of aquatic mammals and fish are within the range of underwater noise generated by the ship propulsion, as shown in Figure 6. Therefore, the emitted noise levels are within the hearing ranges of a series of aquatic mammals which might impact their communication, reproduction, navigation, and even predator avoidance.

There are plenty of sources that may contribute to the noise levels and they also vary according to the operational condition of the ship. For example, when a commercial vessel is at berth, the main sources of noise will be the diesel generators, engine exhaust, the ventilation inlets, and outlets and secondary sources such as pumps and other machinery.

With the same vessel in a navigating condition, other sources must be added and might be more relevant, such as the noise generated by propeller radiating pressure and propeller cavity.
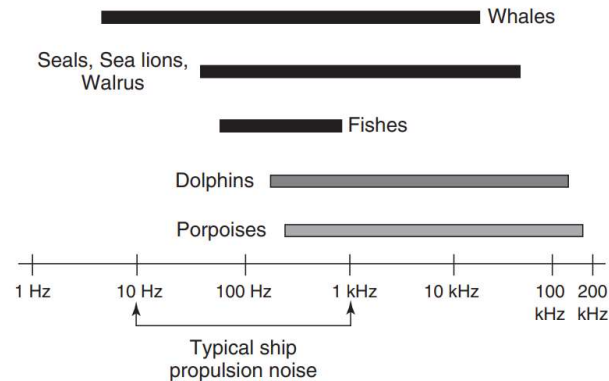
Figure 6. Range of underwater ship noise compared to the hearing range of aquatic animals. Available from https://www.researchgate.net/publication/314277631_Underwater_Noise_from_Large_Commercial_Ships-International_Collaboration_for_Noise_Reduction [Accessed 30 May 2020]

The noise generated by these sources can be transmitted through the walls, frames, and decks, but also the vibrational energy can be transmitted. This latter source usually occurs when the machinery of the vessel is mounted over light foundations and will mostly affect the adjacent compartments, even if there is good acoustic isolation. This type of noise source is referred to as structure-borne noise and it is often generated by induced vibration forces coming from the propeller and the machinery. Figure 7, from [4], exemplifies the chain reaction of the phenomenon in a pleasure boat.

Typically, this occurs at frequencies higher than 1000 Hz, thus, to perform such analysis with a deterministic approach, the element size of the finite element mesh must be refined until there is enough precision to capture the wavelength in higher frequencies. For a structure as large as a commercial vessel, it is clear that the approach is unfeasible due to the increase in computational cost. In addition to this, the relevance of a deterministic approach in a context of high modal density is questionable. Therefore, several other methods have been developed, such as the Statistical Energy Analysis (SEA) - which is the main approach used in this study - the Energy Finite Element Method (EFEM), Energy Flow Analysis (EFA) and Ray Tracing.
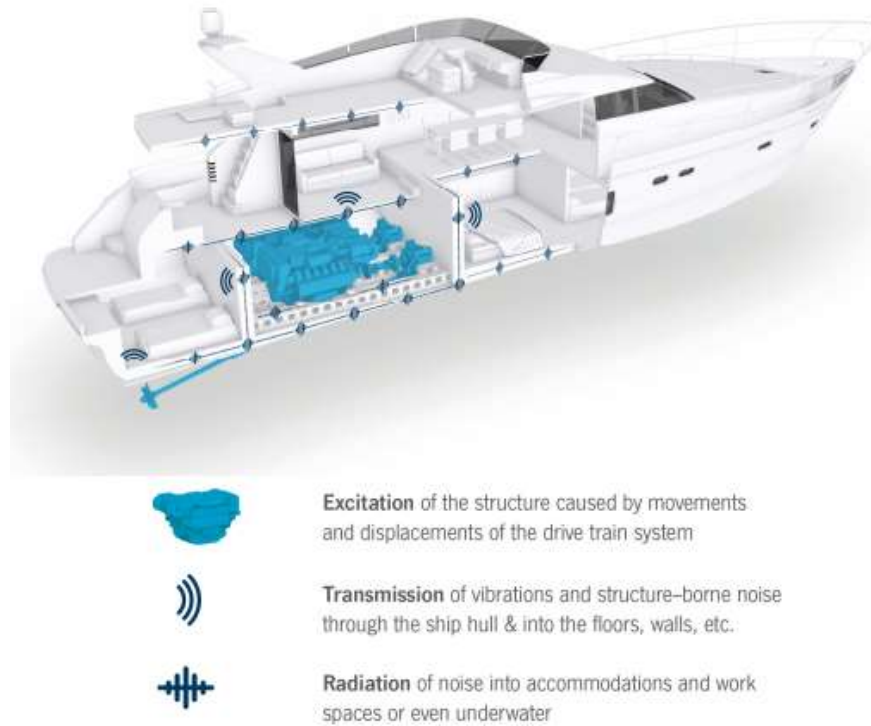
Figure 7. Structure-borne noise on a pleasure boat. Available from http://pub.dega-akustik.de/ICA2019/data/articles/000149.pdf [Accessed 30 May 2020]

1.3 The objective of the Study

As shown above, there are plenty of reasons to perform a vibroacoustic analysis of new designs, not only for projects related to ships and vessels but also for most of the lightweight structures. To do so, many techniques have been researched and widely utilized. One of these techniques is the SEA framework that has already been successfully implemented in the product Actran Virtual SEA developed by the company Free Field Technologies.

From the noise level prediction, the next step is to implement an optimization procedure. With such a tool, it would be desirable to change the mechanical properties of a model and evaluate the effect of the perturbation on its energy levels. If the procedure can be done at a low cost for each iteration, then based on the objectives and constraints of the designer, an optimum configuration can be achieved for an acceptable cost.

Two steps in a Virtual SEA analysis make a straightforward implementation unfeasible: the modal extraction and the assembly of the distribution matrices. These two steps will be discussed in more detail in the next topics.

If these procedures have to be re-performed at each iteration, the implementation of an optimization tool will be computationally expensive, especially with ship models that usually contain hundreds of thousands of modes.

Therefore, the main objective of this study is the development of a framework that changes the mechanical properties of a model, such as the mass, stiffness, and damping, and allows the prediction of the energy levels for the perturbed model based on the nominal modal basis and nominal distribution matrices. If such a procedure is possible, then an optimization script can be developed to test and validate the method.

To do so, an industrial size ship, represented by a finite element mesh, has been provided by the ANAST department of the University of Liège, as shown in Figure 8. The model represents a fraction of the aft part of a RORO vessel. This section of the design would be of particular interest for a vibroacoustic analysis since it is where the engine room is located with many distinct noise sources.

Since a ship structure is composed of many components, for instance: stiffeners, girders, bulkheads, frames, etc; and each of these components will have different cross-sections and plate thickness, it can be very challenging to estimate which components and how they should be modified to achieve a better vibroacoustic behavior, even for an experienced engineer. Thus, the development of such a tool is vital to aid in the assessment of the sensitivity of the model towards the change in its mechanical properties.
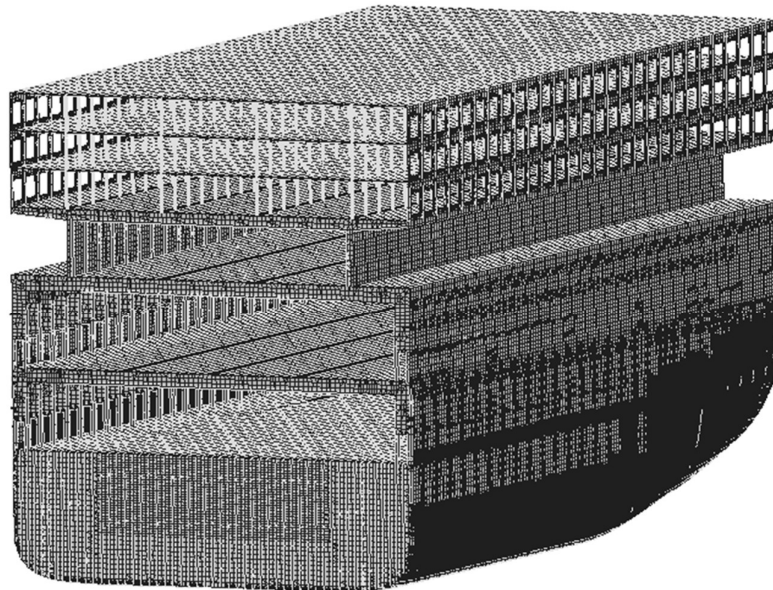
Figure 8. Finite element representation of a RORO vessel

2. ENERGY DISTRIBUTION MODELS

Before introducing the SEA concept, this section explains the concept of finite element energy distributed models, a method used to describe a complex model for high-frequency range problems.

2.1 Introduction

The expressions derived in the next topics are made under the assumption of a system divided into multiple subsystems. It is shown in Figure 9 an example of a system substructured into subsystems where each subsystem is represented by a different color.
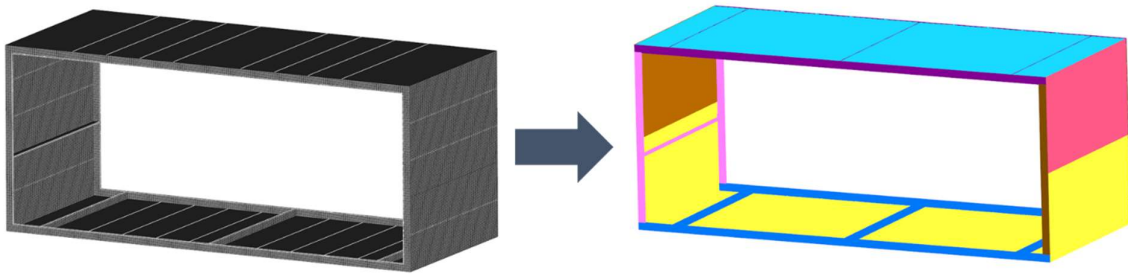
Figure 9. Substructuring example

Also, each subsystem is excited by a random distributed external force and their response is considered linear. In Mace and Shorter (2000) [5], expressions are developed to estimate the energetic values of the subsystems.

2.2 Model Discretization

A structure can be discretized by the finite element method which will define the mass (**M)** and stiffness (**K)** matrix of the system according to the used element type.

As presented by Mace and Shorter (2000) [5], if an external force is applied on an undamped problem, the expression yields

$$\mathbf{M}\ddot{u} + \mathbf{K}u = f^u \tag{2.1}$$

where u represents the nodal displacement vector, $\ddot{u}$ is the nodal acceleration vector and f^u is a nodal force vector. The size of all these vectors is equal to the number of degrees of freedom.

The system parameters can be expressed as a function of the r-subsystem matrices by employing a transformation matrix ($\mathbf{S}_r$). This matrix contains terms that are present in one subsystem, but also terms that are present in more than one subsystem or in no subsystem, which are the terms that will guarantee the coupling and continuity of the model. Thus, the nodal displacement and the matrices of a subsystem are defined as

$$u_r = \mathbf{S}_r u; \quad \mathbf{M}_r = \mathbf{S}_r \mathbf{M}; \quad \mathbf{K}_r = \mathbf{S}_r \mathbf{K} \tag{2.2}$$

If the vector u is known, the kinetic and potential energies are defined as:

$$V = \frac{1}{2} u^T \mathbf{K} u; \quad T = \frac{1}{2} \dot{u}^T \mathbf{M} \dot{u}; \quad V_r = \frac{1}{2} u^T{}_r \mathbf{K}_r u_r; \quad T_r = \frac{1}{2} \dot{u}_r{}^T \mathbf{M}_r \dot{u}_r; \tag{2.3}$$

2.3 Definition of the Distribution Matrices

In a dynamic context, the force f^u is assumed to be time-harmonic (Mace and Shorter, 2000) [5] and expressed by

$$f^u = \mathbf{F}^u e^{i\omega t} \tag{2.4}$$

with the term $\mathbf{F}^u$ being the representation of the complex force amplitudes vector.
The structural, or hysteric, damping is considered based on a constant loss factor η which expresses the frequency dependence behavior. The response of the system is then

$$\mathbf{U} = [\mathbf{K}(1 + i\eta) - \omega^2 \mathbf{M}]^{-1} \mathbf{F}^u \tag{2.5}$$

where the term $1 + i\eta$, often referred to as "complex stiffness", is a combined representation of the stiffness and hysteric damping [6].

Thus, the time-averaged energetic value of the system is defined by

$$V = \frac{1}{2} \Re \left\{ \frac{1}{2} \mathbf{U}^H \mathbf{K} \mathbf{U} \right\} = \frac{1}{4} \mathbf{U}^H \mathbf{K} \mathbf{U}; \quad T = \frac{1}{2} \Re \left\{ \frac{1}{2} (i\omega \mathbf{U})^H \mathbf{M} (i\omega \mathbf{U}) \right\} = \frac{1}{4} \omega^2 \mathbf{U}^H \mathbf{M} \mathbf{U} \tag{2.6}$$

Similarly, the injected and dissipated powers can be expressed by

$$P_{in} = \frac{1}{2} \Re \{ i\omega \mathbf{F}^H \mathbf{U} \}; \quad P_{diss} = \frac{1}{2} \omega\eta \, \mathbf{U}^H \mathbf{K} \mathbf{U} = 2\omega\eta \, V \tag{2.7}$$

From the previous expressions, it is possible to solve the system of equations and estimate the energetic values of the subsystems. Nevertheless, to perform such an analysis, it is necessary to invert the matrix present in Eq. 2.5 for each frequency. Since this matrix is of order equal to the number of degrees of freedom of the system, the process becomes computationally expensive for large and refined finite elements mesh.

As presented by Mace and Shorter (2000) [5], it is more efficient to perform the analysis based on the modal decomposition of the global modes of the system. By this approach, assuming that there are as many modes as degrees of freedom, there will be many non-resonant modes with a reduced contribution to the response that can be neglected, and thus, the analysis is numerically more efficient.

To retrieve the global modes of the system, a modal analysis must be performed. For free-vibration and when neglecting the damping, the generalized eigenproblem equation is defined as

$$\mathbf{K}\boldsymbol{\phi} = \lambda\mathbf{M}\boldsymbol{\phi} \tag{2.8}$$

where λ is a vector that contains the square of the eigenfrequencies (ω) and $\boldsymbol{\phi}$ is the modal matrix that contains the eigenvectors.

This expression must satisfy the M-orthonormality which corrects the lengths of the eigenvectors (Bathe, 2014) [7]. Thus, the following conditions must be satisfied

$$\boldsymbol{\phi}_i^T\mathbf{M}\boldsymbol{\phi}_j = \delta_{ij} \tag{2.9}$$

where δ_{ij} is the Kronecker delta defined by

$$\delta_{ij} = \begin{cases} 0 & if\ i \neq j \\ 1 & if\ i = j \end{cases} \tag{2.10}$$

Multiplying Eq. 2.8 by $\boldsymbol{\phi}^T$ and using the established relation in Eq. 2.9, the following expression is obtained

$$\boldsymbol{\phi}_i^T\mathbf{K}\boldsymbol{\phi}_j = \lambda\delta_{ij} \tag{2.11}$$

Thus, the eigenvectors will also be K-orthogonal and directly proportional to λ. Therefore, Eqs. 2.9 and 2.11 can be re-written as

$$\boldsymbol{\Phi}^T\mathbf{M}\boldsymbol{\Phi} = \mathbf{I}; \qquad \boldsymbol{\Phi}^T\mathbf{K}\boldsymbol{\Phi} = \boldsymbol{\Omega}^2 \tag{2.12}$$

with $\boldsymbol{\Phi}$ being a matrix containing the eigenvectors $\boldsymbol{\phi}$ and $\boldsymbol{\Omega}$ the diagonal matrix containing the eigenfrequencies ω^2.

The modal forces and response are then defined as

$$F_i^y = \boldsymbol{\phi}_i^T\mathbf{F}^u; \qquad Y_i = \alpha_i F_i^y, \qquad i = 1, \dots, m \tag{2.13}$$

with α_i being the modal receptance given by

$$\alpha_i = \frac{1}{\omega_i^2(1 + i\eta) - \omega^2} \tag{2.14}$$

Thus, the response expressed in Eq. 2.5 becomes

$$\mathbf{U} = \boldsymbol{\Phi}\mathbf{Y} \tag{2.15}$$

with $\mathbf{Y}$ being the vector of the modal responses.

Mace and Shorter (2000) [5] define the time-averaged kinetic and potential energies of the system as the sum of the energies of each mode, according to the previous mass and stiffness matrices definition

$$V = \frac{1}{4} \sum_i \omega_i^2 |Y_i|^2; \quad T = \frac{1}{4} \omega^2 \sum_i |Y_i|^2 \tag{2.16}$$

Nevertheless, these expressions are different for each of the subsystems since the Eq. 2.12 is only valid for the global matrices of the system. The stiffness and mass distribution matrices will be a projection over the mode shapes, such as

$$K_r = \mathbf{\Phi}^T \mathbf{S}_r^T \mathbf{K_r} \mathbf{S}_r \, \mathbf{\Phi}; \quad M_r = \mathbf{\Phi}^T \mathbf{S}_r^T \mathbf{M_r} \mathbf{S}_r \, \mathbf{\Phi} \tag{2.17}$$

The time-averaged kinetic and potential energies of the subsystems are then given by:

$$V_r = \frac{1}{4} \mathbf{Y}^H K_r \mathbf{Y}; \quad T_r = \frac{1}{4} \omega^2 \mathbf{Y}^H M_r \mathbf{Y} \tag{2.18}$$

2.4 Spatially Distributed Excitations

The spatial distributed excitations can be either coherent or incoherent. In the case of a coherent excitation over broadband, the energetic expression (Mace and Shorter, 2000) [5] of the system is defined by

$$V = \frac{1}{4} \sum_m \psi_{a,mm} \omega_m^2 |\alpha_m|^2 \, ; \ T = \frac{1}{4} \omega^2 \sum_m \psi_{a,mm} |\alpha_m|^2 \, ; \ P_{in} = \frac{1}{2} \Re \left\{ i\omega \sum_m \psi_{a,mm} \alpha_m \right\} \tag{2.19}$$

where $\psi_{a,mm}$ is the modal distribution force term and it corresponds to the intensity that the mode m will be excited based on the mode shape of the system. Similarly to the development of the Eqs. 2.16 and 2.18, the kinetic and potential energies of the subsystems are described as

$$V_r = \sum_{m,p} (\psi_{a,mp} K_{r,mp}) \Gamma_{mp} \, ; \quad T_r = \sum_{m,p} (\psi_{a,mp} M_{r,mp}) \omega^2 \Gamma_{mp} \tag{2.20}$$

with Γ_{mp} being a frequency-dependent term

$$\Gamma_{mp} = \frac{1}{4} \alpha_m^* \alpha_p \tag{2.21}$$

From a computational point of view, only the term Γ_{mp} in Eq. 2.20 is to be evaluated for each frequency since the terms between the parenthesis only need to be calculated once (Mace and Shorter, 2000) [5].

In the case where there are incoherently distributed forces, or rain-on-the-roof excitations, and in the particular case of spatially delta-correlated loads, the input forces are proportional to the modal mass of the determined subsystem, at the specific frequency. Thus, the expression (Mace, 2003) [8] of the subsystem injected power will be defined by

$$E[P_{in,r}] = S_f \frac{\pi}{2} n_r(\omega) \qquad (2.22)$$

where S_f is the spectral density, $n_r(\omega)$ is the modal density of the subsystem r at the frequency ω and E[.] represents is the asymptotic average.

Also, from Eq. 2.22, it follows that the modal distribution force will be proportional to the fractional modal density of the subsystem, which is the ratio of the subsystem modal density by the total modal density of the system. Thus, the following expression is defined

$$E[\psi_{a,mm}] = \frac{n_r}{n_{total}} \qquad (2.23)$$

Therefore, this implies that the modal forces applied to a subsystem will be proportional to its mass distribution matrix since both are defined by the modal densities, according to Appendix A in [8].

2.5 Averaged Frequencies

Considering the previous case of spatial incoherent delta-correlated rain-on-the-roof excitation and by assuming that the power spectral density and the loss factor terms are constant or known functions of frequency, for a light damping assumption, the energy terms for a frequency range Ω within a broadband B are:

$$\bar{V} = \left(\frac{S_f}{4B}\right) \sum_m \omega_m^2 \, \psi'_{s,mm} J_{1,m}, \quad J_{1,m} = \int_\Omega |\alpha_m|^2 d\omega,$$

$$\bar{T} = \left(\frac{S_f}{4B}\right) \sum_m \psi'_{s,mm} J_{2,m}, \quad J_{2,m} = \int_\Omega \omega^2 |\alpha_m|^2 d\omega,$$

$$\bar{P}_{in} = \left(\frac{S_f}{2B}\right) \sum_m \psi'_{s,mm} J_{3,m}, \quad J_{3,m} = \int_\Omega \mathcal{Re}\{i\omega\alpha_m\}d\omega, \qquad (2.24)$$

$$\bar{V}_b = \left(\frac{S_f}{4B}\right) \sum_{m,p} \psi'_{s,mp} K_{r,mp} J_{4,mp}, \quad J_{4,mp} = \int_\Omega \alpha_m^* \alpha_p d\omega,$$

$$\bar{T}_b = \left(\frac{S_f}{4B}\right) \sum_{m,p} \psi'_{s,mp} M_{r,mp} J_{5,mp}, \quad J_{5,mp} = \int_\Omega \omega^2 \alpha_m^* \alpha_p d\omega.$$

where *r* represents the terms of the response of the coupled subsystem and J are the frequency integrals.

These frequency integrals with index 1,2 and 3 are generally small except for the resonant modes while 4 and 5 indexes are also small except for the overlapping modes. These expressions can be developed in closed-form and are demonstrated by Mace and Shorter (2000) [5].

2.6 Actran Energy Analysis Workflow (ACTRAN/ EA)

The Actran Energy Analysis (EA) workflow implements the concept of energy distributed models to perform energetic post-processing of large-scale finite element models.

The system is divided by *r*-subsystems, each of them defined by a set of elements called element patch (P_k) [9]. For example, in Figure 10 the system has been substructured into subsystems. For the subsystem represented in yellow, it is composed of three elementary patches: the lower plate, part of the side plate, and the bottom beams.
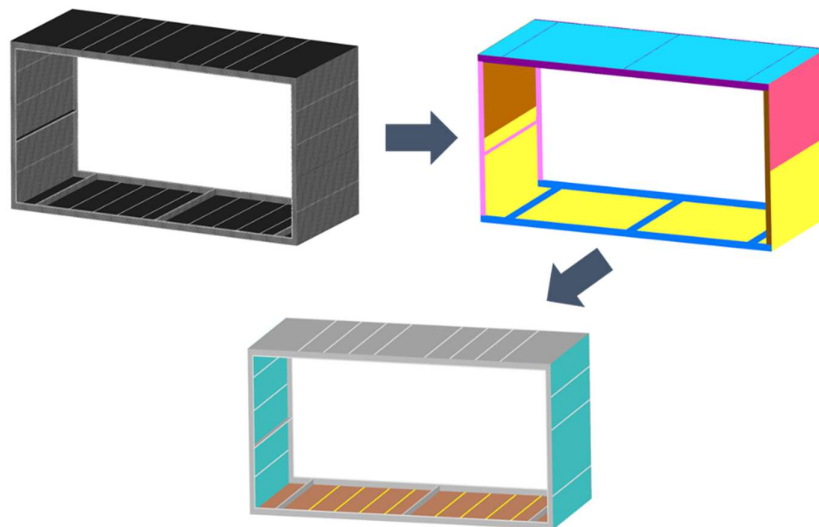
Figure 10. Example of the substructuring and elementary patch

The properties of the elementary patches are a projection of the modal basis (Φ) of the stiffness and mass matrices on its composing elements, just as defined in the Eq. 2.17. Once these matrices are defined, the energetic quantities can be calculated. The definition of the subsystem distribution matrices and their energetic values will be used to perform the Virtual SEA analysis.

2.6.1   Distribution matrices assembly

Since each element patch contains a series of elements, its stiffness and mass distribution matrices are assembled from the modal projection of the mass and stiffness of the contained elements, therefore the expressions can be defined as:

$$K_k = \mathbf{\Phi}^T \cdot \sum_{e \epsilon P_k} K_e \cdot \mathbf{\Phi}; \qquad M_k = \mathbf{\Phi}^T \cdot \sum_{e \epsilon P_k} M_e \cdot \mathbf{\Phi} \qquad (2.25)$$

where K_e and M_e are respectively the stiffness and mass elementary matrices, $\mathbf{\Phi}$ is the modal basis of the system. Denoting by $\mathbf{K_k}$ and $\mathbf{M_k}$ the assembled stiffness and mass matrices on the element patch, the distribution matrices are:

$$K_k = \Phi^T \cdot \mathbf{K_k} \cdot \Phi; \qquad M_k = \Phi^T \cdot \mathbf{M_k} \cdot \Phi \qquad (2.26)$$

Similarly to the element patch assembly, the global distribution matrices (K and M) can be defined as the sum of each element patch distribution matrices which yields the same expression as defined in Eq. 2.12.

3. STATISTICAL ENERGY ANALYSIS (SEA)

The Statistical Energy Analysis (SEA) is a framework typically used to solve vibroacoustic problems in high-frequency ranges. The approach considers a structure, referred to as a system, divided into its components, referred to as subsystems. By injecting a known power into the system and calculating the energy levels of the subsystems, a linear system of equations can be solved to retrieve the parameters of the system, referred to as SEA parameters, which will correspond to its response function. From these energy levels, information such as averaged sound pressure, stress, and strain can be retrieved. The next sections discuss the SEA theory in more detail.

3.1 Introduction

The SEA framework started to be developed in the early *'60s* by Lyon and Maidanik (1962) [10], and Smith (1962) [11]. At that time, lightweight structures, such as airplanes and automotive vehicles, became more frequent and in these cases, it is known that structure-borne noise can be a major concern, thus, the demand for the assessment of the noise levels increased.

The SEA concept considers that the vibrational energy of a structure will be diffused to its components, similarly as it occurs with heat diffusion. By developing an efficient coupling of the components of a structure, the method can efficiently predict the vibrational energy of the model, and therefore predict with accuracy the noise propagation of the design. Thus, the framework became popular in the industry.

Traditionally, there are two different applications for the SEA framework: the experimental SEA and the analytic SEA. The first approach applies an injected power to a physical model or prototype and by measuring the response of the components, the SEA parameters are calculated economically and with good accuracy. The second method tries to evaluate the SEA parameters by analytical expressions at an early design phase, allowing to predict and identify potential noise-related issues. For complex structures, such as airplanes and ships, typically it is difficult to solve vibroacoustic problems after the design has been finalized. Any design modification will mostly impact other engineering fields and possibly generate other issues. The SEA framework offers a reliable method that can be implemented in the early design phase.

3.2 Energy Exchange of Coupled Subsystems

Before addressing the SEA expressions, it is important to understand the concept behind the diffusion of vibrational energy between distinct subsystems, as explained by De Langhe (1996) [1]. Expressions are derived for the energy exchange of two subsystems with multiple degrees of freedom. The subsystems are excited by a random force and they respond according to their excitation and the interaction between them that is transmitted by their coupling.

Each subsystem contains a modal basis of N modes within the frequency range of interest and with modes that are considered to be equally spaced over the frequency interval and all modes of a subsystem are considered equally energetic. Furthermore, the applied damping is assumed to be similar for both subsystems.

As a result, a mode of one of the subsystems is connected to all the other modes of the adjacent subsystem, but it is not connected with the modes of the same subsystem. This is exemplified in Figure 11.
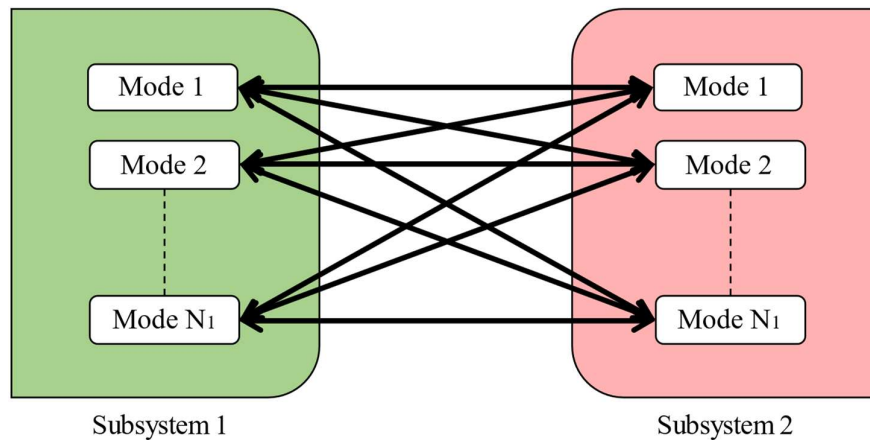
Figure 11. Interaction of the modes between coupled subsystems

For a pair of oscillators that are excited with white noise, the time-averaged energy flow can be described by their vibrational energy difference, yielding

$$E_{1,1} = E_{2,1} = E_{N_1,1} = \frac{E_1}{N_1}; \qquad E_{2,2} = E_{1,2} = E_{N_2,2} = \frac{E_2}{N_2} \qquad (3.1)$$

For a pair of oscillators that are excited with white noise, the time-averaged energy flow can be described by their vibrational energy difference, yielding

$$P_{12} = g_{12}(E_1 - E_2) \qquad (3.2)$$

where g_{12} represents a parameter that depends on the mechanical properties of the system.

As explained by De Langhe (1996) [1], the total energy flow of the system is the sum of the energy flow for each mode pairing. Thus, the net energy flow is described by

$$P_{12} = \langle g \rangle N_1 N_2 \left(\frac{E_1}{N_1} - \frac{E_2}{N_2} \right) \tag{3.3}$$

with $\langle g \rangle$ an average value over the desired frequency range of study.

The previous expression shows that the energy flow is proportional to the difference of the modal energies if the expression is averaged over time within a frequency range of interest Δf. Eq. 3.3 then becomes

$$P_{12} = \omega (\eta_{12} E_1 - \eta_{21} E_2) \tag{3.4}$$

with the reciprocity relation

$$n_1 \eta_{12} = n_2 \eta_{21} \tag{3.5}$$

with ω the band center frequency, n_1 and n_2 the modal densities of subsystems one and two, and η_{12} and η_{21} an important SEA value, the coupling loss factors (CLF). The modal densities and CLF expressions are respectively

$$n_1 = \frac{N_1}{\Delta f}; \quad n_2 = \frac{N_2}{\Delta f} \tag{3.6}$$

$$\eta_{12} = \frac{\langle g \rangle n_2 \Delta f}{\omega}; \quad \eta_{21} = \frac{\langle g \rangle n_1 \Delta f}{\omega} \tag{3.7}$$

Since the terms η_{12} and η_{21} are proportional to the modal densities, and therefore not identical, the symmetry of the energy flow is lost. This can be understood by analyzing Eq. 3.4 by terms, the first $\omega \eta_{12} E_1$ represents the energy lost by subsystem 1 due to the coupling with subsystem 2 and $\omega \eta_{21} E_2$ will represent the energy lost by subsystem 2 due to the coupling with subsystem 1.

By considering the injected and dissipated power in the energy balance, the terms related to the second will be defined as $\omega \eta_1 E_1$ and $\omega \eta_2 E_2$, with η_1 and η_2 being the terms that represent the damping of each subsystem, thus these terms are referred to as damping loss factors (DLF).

3.3 Generalized SEA Expressions

Once the vibrational energy flow between the subsystems is understood, the equations defined in the previous section can be extended for a system composed of multiple modal-represented subsystems.

The time-averaged energy flow between two coupled subsystems can be generalized as the energy exchange between the subsystem i to subsystem j.

$$P_{ij} = \omega g_{ij} \left(\frac{E_i}{N_i} - \frac{E_j}{N_j} \right) \tag{3.8}$$

Analogously, equations 3.4 and 3.5 can be written as

$$P_{ij} = \omega \left(\eta_{ij} E_i - \eta_{ji} E_j \right) \tag{3.9}$$

$$n_i \eta_{ij} = n_j \eta_{ji} \tag{3.10}$$

Considering the time-averaged dissipated power as

$$P_{i,diss} = \omega \eta_i E_i \tag{3.11}$$

Based on the previous expressions, it is possible to analyze a structure composed of multiple subsystems and establish a power balance, as seen in Figure 12. For a given injected power in subsystem i, its modal response will excite the modes of the coupled subsystems and with each subsystem dissipating energy due to the damping.
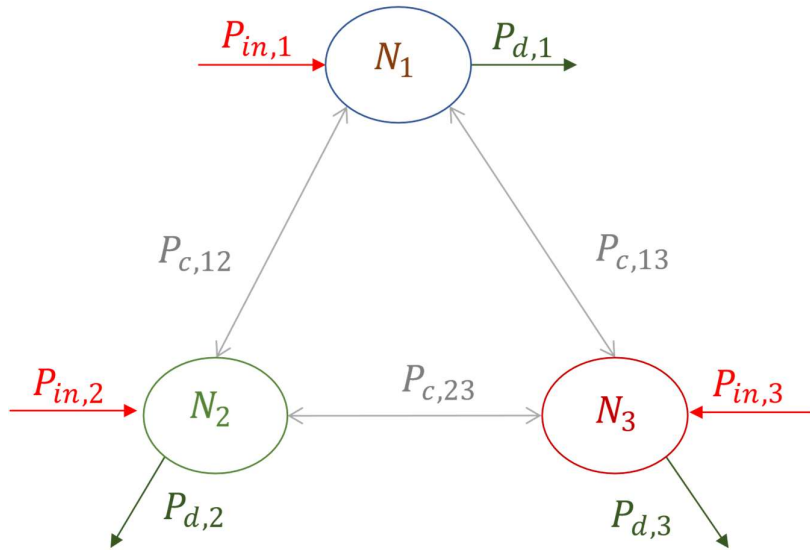
Figure 12. The power balance of a system portioned into subsystems

For a given subsystem i, the generalized time-averaged power balance equation will be equivalent to its dissipated power and the transmitted power to the coupled subsystem, such as

$$P_{in,i} = P_{d,i} + \sum_{\substack{j \neq i}}^{r} P_{c,ij}; \quad i = 1, \dots, r \tag{3.12}$$

By considering Eqs.3.9 and 3.11, the expression can be re-written as:

$$P_{in,i} = \omega \eta_{ii} E_i + \sum_{j \neq i}^{r} \omega \left(\eta_{ij} E_i - \eta_{ji} E_j \right) \tag{3.13}$$

By considering the SEA reciprocity, expressed in Eq. 3.10, the power balance of the system can be written in a matrix form

$$\omega \begin{pmatrix} \left(\eta_{11} + \sum_{i \neq 1}^{r} \eta_{1i} \right) n_1 & -\eta_{12}\, n_1 & \cdots & -\eta_{1r}\, n_1 \\ -\eta_{21}\, n_2 & \left(\eta_{22} + \sum_{i \neq 2}^{r} \eta_{2i} \right) n_2 & \ddots & \vdots \\ \vdots & \ddots & \ddots & \vdots \\ -\eta_{r1}\, n_r & \cdots & \cdots & \left(\eta_{rr} + \sum_{i \neq r}^{r} \eta_{ri} \right) n_r \end{pmatrix} \begin{Bmatrix} E_1/n_1 \\ E_2/n_2 \\ \vdots \\ E_r/n_r \end{Bmatrix} = \begin{Bmatrix} P_1 \\ P_2 \\ \vdots \\ P_r \end{Bmatrix} \tag{3.14}$$

It is also possible to write the power balance in a compact matrix form

$$\mathbf{P} = \omega[\boldsymbol{\eta}]\mathbf{E} \tag{3.15}$$

with the SEA parameters, CLFs and DLFs expressed respectively as

$$\eta_{ij} = -[\eta]_{ji} \tag{3.16}$$

$$\eta_i = \sum_{i=1}^{r} [\eta]_{ij} \tag{3.17}$$

If the SEA matrix $\boldsymbol{\eta}$ is known, then it is possible to predict the global behavior of the structure for any given injected power $\mathbf{P}$ by simply performing an inexpensive matrix inversion,

$$\mathbf{E} = \frac{1}{\omega}[\boldsymbol{\eta}]^{-1}\mathbf{P} \tag{3.18}$$

Nevertheless, the SEA method requires that some assumptions are complied to achieve a feasible result, and often it is difficult to validate a SEA model. These assumptions and difficulties will be addressed in section 3.8.

3.4 Calculation of the SEA Matrix

As seen in section 3.3, the SEA matrix is essential to calculate the global energetic behavior of a system. As reviewed by De Langhe (1996) [1], two main approaches were developed to calculate the SEA matrix: the analytic SEA and the experimental SEA. Both exists since the beginning of the SEA theory, although the second approach only became popular more recently.

3.4.1 Analytic SEA

Although the SEA expression (Eq. 3.8) in the previous section is based on a modal representation of the system, the analytical SEA considers a different representation by the wave approach. In this method, the system will also be divided into subsystems, but instead of representing the structure's components, in the wave approach, each subsystem will correspond to a wave type according to the needs of the analyst. Therefore, a component of a structure might be represented by longitudinal, transverse, flexural waves, etc, and each of these waves will be considered as a distinct subsystem. Such a division is necessary since each wave type will yield different analytical expressions.

The coupling loss factors will be evaluated analytically according to the ratio of the energies transmitted by the dissipated and incoming waves in the same subsystem. Thus, this will imply that there are only non-zero CLFs between physically connected components and the SEA matrix will be sparse. Also, these characteristics of the CLFs have a strong physical significance since there should not be an energy exchange between components that are not physically coupled. In Eq. 3.18 it is seen that the SEA matrix must be inverted to obtain the energy level of the analyzed system, and since the matrix is of order equals to the r-subsystems, its inversion is inexpensive. For these reasons, the analytical approach was widely accepted by the scientific community since its development and many of the SEA software is based on this approach.

Nevertheless, the implementation of the method also relies on existing analytical expressions for a given geometry. Thus, complex structures, such as a combustion engine, can hardly be represented by this method without making great geometry simplifications. Additionally, it is often a complex task to determine the partitioning of the subsystems and validate it by guaranteeing that the model does not violate any SEA assumptions. Because of these limitations, for many practical models, the analytical method is restricted to early design phases on a simplified design.

3.4.2 Experimental SEA

Since representing complex geometries with the analytical SEA approach usually is not feasible, the experimental SEA appears as an alternative to measure the energy flow *in situ* of a model or prototype and quickly retrieve the SEA matrix.

At the beginning of its development, due to the appearance of negative CLFs terms between non-physically coupled subsystems, the method suffered credibility issues as it is unfeasible to establish a physical correlation. Nevertheless, studies applying the experimental method could achieve good approximations of the structure response, even with negative CLFs terms.

Another drawback of the method is that since it requires a prototype to be performed, it cannot be implemented at the beginning of a design cycle. Also, it requires that the energy inputs and measurements are large enough so that a good precision of the SEA matrix is obtained. Thus, it is evident that large structures such as ships and airplanes will require a large amount of time and human resources to perform these measurements. Additionally, the instruments used during the measurements should be precise enough and the settlement of the structure must be sufficient to avoid adding imprecisions to the values calculated.

3.5 The SEA Parameters

The SEA method expresses the energetic value exchange between a system divided into components. Therefore, the key to a successful analysis is correctly computing the input energy, the energy levels of each subsystem, their dissipated energy, and transmitted energy.

As seen through Eqs. 3.9-3.11, there are some important parameters involved in the power balance expressions. In the following sections, the Damping Loss Factors (DLF), Coupling Loss Factors (CLF), and the subsystem's modal densities will be briefly explained, as defined by De Langhe (1996) [1], while their calculation will be shown in section 3.6.

3.5.1 Damping Loss Factors (DLFs)

The DLFs in a SEA model represent the coefficients related to the energy dissipated by the subsystem according to the applied damping. Thus, these can be defined by the ratio of the dissipated energy divided by the energy level of the subsystem and the center frequency.

Different types of damping can be considered within the SEA framework, such as the structural, acoustic radiation, non-linear, and local internal damping. The structural damping is related to the mechanical properties of the model; the acoustic radiation represents the losses of the energy transmitted through the surface of the structure to the attached medium.

For instance, an air cavity or unbounded water domain; the non-linear damping is usually related to the damping of the coupling interfaces and the local internal damping is due to inner friction.

It is important that the damping mechanisms are independent. The total damping of a subsystem can then simply be calculated as the sum of the different contributions.

It is important to state that the damping mechanisms will be independent, thus the total damping of a subsystem can be simply calculated by the sum of the different contributions.

However, some simplifications can be assumed, for instance, the damping due to the interfaces can usually be neglected at higher frequencies. This will also be part of one of the SEA assumptions that are discussed in section 3.8.

Also, depending on the model, there might be different dominant damping mechanisms. For instance, a lightweight structure with poor damping material application will mostly be dominated by the acoustic radiation.

3.5.2 Coupling Loss Factors (CLFs)

The CLFs are related to the vibrational energy exchange between the subsystems. The evaluation of these coefficients has been widely investigated over the years since different methodologies to calculate them, achieve different results. This topic is discussed in more detail in section 3.8.

The main difficulties to calculate these parameters are related to the complexity of the junctions and their mechanical properties. As seen previously, the analytical method can only be accurate for simple geometries, while the experimental method can handle more complex couplings. However, the latter will present results of CLFs between non-coupled subsystems and even negative values, which do not have a physical representation.

3.5.3 Modal Densities

The modal densities have an important role in the reciprocity relation (Eq. 3.10) and express the available resonant modes that store energies and the modes that transmit energies to the other subsystems. In practice, it will determine the dominant paths of the energy flow, since the vibrational energy will flow from the highest modal density in the model to the lowest.

The magnitude of the modal densities of a subsystem can be calculated by the number of resonant modes per unit frequency in a narrow or broadband. This procedure can be done experimentally or by analytical expressions for simplified geometries.

3.6 The Power Injection Method (PIM)

The Power Injected Method (PIM) is one of the experimental strategies used to calculate the SEA matrix. By measuring the input power that subsystems are submitted and their kinetic energy response, an estimation of the total energy of the system is achieved. The results of the method are reliable as long as the averaged energies are performed with a large modal basis.

The method described in this section is derived from De Langhe (1996) [1] which he named the normalized energy inversion method and will be the base of the Actran Virtual SEA implementation.

3.6.1 Expressions for two coupled subsystems

To exemplify a simple application of the PIM, as done in item 3.2, two coupled subsystems are considered as shown in Figure 13,
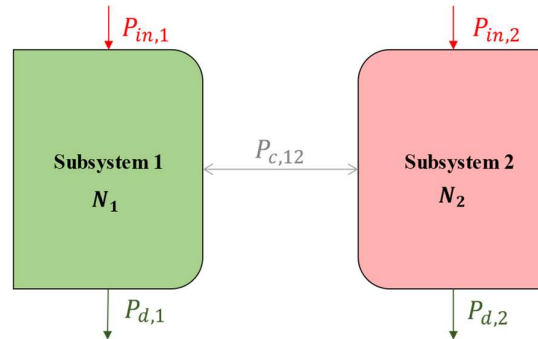
Figure 13. PIM representation of a two-subsystem SEA model

For this simple example, it is possible to write the power balance of the system expressed in the Eq. 3.15 as

$$\begin{bmatrix} P_1 \\ P_2 \end{bmatrix} = \omega \begin{bmatrix} \eta^o_{11} & \eta^o_{12} \\ \eta^o_{21} & \eta^o_{22} \end{bmatrix} \begin{bmatrix} E_1 \\ E_2 \end{bmatrix} \tag{3.19}$$

In the PIM, one subsystem is excited at a time and the kinetic energies of all subsystems are measured experimentally.

Thus, for the case of two subsystems, the power balance of the system expresses the following load cases: the injected power frequency averaged and the energy levels of each subsystem frequency and spatially averaged.

$$\begin{bmatrix} P_1 \\ 0 \end{bmatrix} = \omega \begin{bmatrix} \eta^o_{11} & \eta^o_{12} \\ \eta^o_{21} & \eta^o_{22} \end{bmatrix} \begin{bmatrix} E_{11} \\ E_{21} \end{bmatrix}; \qquad \begin{bmatrix} 0 \\ P_2 \end{bmatrix} = \omega \begin{bmatrix} \eta^o_{11} & \eta^o_{12} \\ \eta^o_{21} & \eta^o_{22} \end{bmatrix} \begin{bmatrix} E_{12} \\ E_{22} \end{bmatrix} \qquad (3.20)$$

By combining these two expressions, a linear system of equations can be expressed as

$$\begin{bmatrix} P_1 & 0 \\ 0 & P_2 \end{bmatrix} = \omega \begin{bmatrix} \eta^o_{11} & \eta^o_{12} \\ \eta^o_{21} & \eta^o_{22} \end{bmatrix} \begin{bmatrix} E_{11} & E_{12} \\ E_{21} & E_{22} \end{bmatrix} \qquad (3.21)$$

Since the injected power and the energy levels are known, the inverse of the matrix η^0 can be calculated by rearranging the power balance equation and computing it term by term, represented by $\eta^{o'}_{ij}$ in the equation below

$$\eta^{o'}_{ij} = \omega \frac{E_{ij}}{P_j} \qquad (3.22)$$

where j is the index of the excited subsystem and i the remaining subsystems.

Therefore, the matrix η^0 will be retrieved as

$$[\eta^0] = \begin{bmatrix} \eta^o_{11} & \eta^o_{12} \\ \eta^o_{21} & \eta^o_{22} \end{bmatrix} = \begin{bmatrix} \eta^{o'}_{11} & \eta^{o'}_{12} \\ \eta^{o'}_{21} & \eta^{o'}_{22} \end{bmatrix}^{-1} \qquad (3.23)$$

The terms that are contained within the matrix η^0 are loss factors related to each subsystem. Therefore, by inverting $[\eta^0]^{-1}$ the SEA parameters are retrieved, with η^o_{11} and η^o_{22} corresponding to damping terms and η^o_{12} and η^o_{21} the coupling terms. Once these values are known the SEA matrix can be composed and defining the DLFs and CLFs by

$$[\eta] = \begin{pmatrix} \eta^o_{11} + \sum_{i \neq 1}^{r} \eta^o_{1i} & -\eta^o_{12} \\ \\ -\eta^o_{21} & \eta^o_{22} + \sum_{i \neq 2}^{r} \eta^o_{2i} \end{pmatrix} \qquad (3.24)$$

3.6.2 Generalized expressions

Analogously to the previous section, the PIM method can be extended to a system composed of r-subsystems which will correspond to most of the practical applications. As the injected power is injected at one a subsystem at a time, there will be a linear system composed of r-equations, such as

$$
\begin{bmatrix} P_1 \\ 0 \\ \vdots \\ 0 \end{bmatrix} = \omega[\eta^o] \begin{bmatrix} E_{11} \\ E_{21} \\ \vdots \\ E_{r1} \end{bmatrix} ; \quad \begin{bmatrix} 0 \\ P_2 \\ \vdots \\ 0 \end{bmatrix} = \omega[\eta^o] \begin{bmatrix} E_{12} \\ E_{22} \\ \vdots \\ E_{r2} \end{bmatrix} ; \quad \begin{bmatrix} 0 \\ 0 \\ \vdots \\ P_r \end{bmatrix} = \omega[\eta^o] \begin{bmatrix} E_{1r} \\ E_{2r} \\ \vdots \\ E_{rr} \end{bmatrix} \tag{3.25}
$$

Then, these can be assembled and represented in a matrix form, such as

$$
\begin{bmatrix} P_1 & 0 & \cdots & 0 \\ 0 & P_2 & 0 & 0 \\ \vdots & \vdots & \ddots & \vdots \\ 0 & 0 & 0 & P_r \end{bmatrix} = \omega[\eta^o] \begin{bmatrix} E_{11} & E_{12} & \cdots & E_{1r} \\ E_{21} & E_{22} & \ddots & E_{2r} \\ \vdots & \vdots & \ddots & \vdots \\ E_{r1} & E_{r2} & \cdots & E_{rr} \end{bmatrix} \tag{3.26}
$$

By retrieving the terms of the matrix $[\eta^o]$ with the procedure explained in the Eqs. 3.22 and 3.23, the generalized SEA matrix composition can be calculated

$$
[\eta] = \begin{pmatrix} \eta^o{}_{11} + \sum_{i \neq 1}^{r} \eta^o{}_{1i} & -\eta^o{}_{12} & \cdots & -\eta^o{}_{1r} \\ -\eta^o{}_{21} & \eta^o{}_{22} + \sum_{i \neq 2}^{r} \eta^o{}_{2i} & \ddots & \vdots \\ \vdots & \ddots & \ddots & \vdots \\ -\eta^o{}_{r1} & \cdots & \cdots & \eta^o{}_{rr} + \sum_{i \neq r}^{r} \eta^o{}_{ri} \end{pmatrix} \tag{3.27}
$$

It is possible to observe that the SEA reciprocity equation (Eq. 3.10) has not been considered in any of the equations related to the PIM. Thus, the modal densities of each subsystem do not have to be calculated to implement this framework. Unlike the analytical method, where all types of waves can be considered, in the experimental PIM, due to the instruments utilized to measure the energies, only bending waves are taken into account since the method measures the kinetic energies. However, in the Virtual SEA, all wave types can be considered, as the method is able to measure the total energy of the model.

3.7 Energy Averaging

Unlike the deterministic approach where local values of displacement, velocity, and accelerations are calculated for specific locations and frequency ranges, the SEA approach calculates averaged energies that represent the global behavior of the system within the frequency range of interest. Thus, there are different average that can be performed such as time, frequency, spatial, and ensemble averaging (De Langhe, 1996) [1].

The time- and frequency-averaging are present in the assumptions of the method's expressions, so this type of averaging does not impose restrictions on its implementation. Thus, it is assumed that the excitations applied to the model are long enough to reduce variations of a time-averaging and a large number of modes within the frequency range of analysis, for a frequency-averaging.

Since the global energy levels of the structure are the goal of the SEA method, these energies must be integrated within the respective subsystems. As a consequence, it is not possible to assess the local values of stress or strain. Nevertheless, these averages will retrieve a good approximation of the global energies as the frequency is increased and the oscillatory movement is diminished.

Lastly, the ensemble averages are related to testing a population of identical systems and evaluating its mean response and variance. In a SEA aspect, instead of analyzing identical systems, the statistical analysis can be understood over the frequencies of one system and relate these frequencies with ensemble quantities. Thus, to some extent, the results of the frequency and space averaging will provide values close to the ergodic mean.

3.8 SEA Assumptions

Due to the different values achieved with the analytical and experimental method, the conditions of validity of a SEA model have been extensively researched. As a result of these extensive works, some well-established conditions must hold to obtain a valid SEA model.

As explained previously, the SEA method is based on the modal transmission between the subsystems and their dissipated power, as expressed in Eqs. 3.9 and 3.11. The expression of the dissipated power is following the classical mechanics, however, the expression describing the modal energy flow requires that a series of conditions are complied to be valid.

This condition, often referred to as Coupling Power Proportionality (CPP), implies that the coupling between the subsystems must be weak. This means that the damped energy will be higher than the transmitted energy.

This weak coupling is important to adjust the energy flow in a multiple subsystem configuration. However, in practice, it is often not evident whether the coupling between the subsystems is weak or not, and verification of the CLFs and DLFs ratio should be performed, with a value less than one. From the wave approach perspective, discontinuities related to high impedance or internal damping can be associated with weakly coupled subsystems.

In addition, the input power must be uncorrelated, which means that non-linear terms will not be introduced to the energy balance equations since they are constructed upon the linearity assumption. Also, the natural frequencies must be distributed equally over the frequency range of the analysis and the vibrational energy must be equally distributed over the modes of a subsystem. This implies that the subsystems will be similar enough to hold the assumption which will hardly be feasible in practical applications, in which cases the assumption will be violated to some extent.

3.8.1 The "quasi-SEA" and "proper-SEA" matrices

In the context of energy distributed models, Mace (2003) [8] establishes that there are two necessary conditions and a series of desirable conditions that if complied will characterize the SEA matrix as a "proper-SEA" matrix, while, if only the two necessary conditions are valid, the SEA matrix will be considered as a "quasi-SEA" matrix.

In energy distribution models, the assumptions of uncorrelated forces and linearity are already attended since they are assumed to develop the expressions of the method. Thus, the two required conditions to ensure the conservation of energy are: the sum of the *rth* column of the SEA matrix must be equal to $\omega\eta_r$ and its off-diagonal terms must satisfy the reciprocity relation (Eq. 3.10).

However, the calculated SEA matrix should also follow a series of desirable conditions to guarantee the validity of the coupling power proportionality. For instance, the CLFs of the subsystems that are not physically connected should be zero, all of them should be positive and independent from the DLFs. In addition, the CLFs must be defined only by the junction between the connected subsystems and its values must not be influenced by the properties of unattached subsystems.

If any of these conditions do not hold, the SEA matrix will contain non-zero indirect CLF between uncoupled subsystems which does not imply that there is an energy exchange between them, these are only additional terms that ensure the energy conservation of the model since the SEA assumptions were violated at some extent. Nevertheless, it is still possible to perform a SEA-like analysis with a "quasi-SEA matrix" and achieve reliable results.

3.8.2 SEA-like matrices validity condition

Mace (2003) [8] also has shown that SEA-like models are possible under certain conditions, even if some SEA assumptions are violated. This is possible since the SEA parameters describe a single system over a frequency range of interest and will be different from an ensemble average.

Besides, it might be the case that even for an ensemble average, the model does not attend all the necessary and desired conditions or the partial conditions that would classify it as a SEA-like mode, therefore, it might be the case which it does not hold the coupling power proportionally invalidating the model.

In the case of a "quasi-SEA" matrix, the reciprocity condition might be attended if there are enough well-characterized modes within the frequency range of interest so that the averaged energies are approximated to the expected values. Thus, it might be acceptable that a "quasi-SEA" matrix contains indirect CLFs, these might be negative. The terms η_{ij} and η_{ji} depend mostly on the global parameters of the system and not the local properties of the subsystems. Finally, the CLFs will depend on the DLFs. Therefore, the coupling power proportionality will comply if these conditions are considered.

3.9 Subsystem Partitioning

The division of a global system into a subsystem is not a straightforward task and there are no clear guidelines on how the partitioning of a model should be performed. The defined subsystem might violate some requirements for a SEA or SEA-like model. For example, the presence of a strong coupling that does not fulfill the coupling power proportionality condition. Thus, this step of the framework is possibly the most important and heavily relies on the experience of the engineer.

Nevertheless, there are two main guidelines to aid in the definition of these subsystems, according to De Langhe (1996) [1]. The first is that the modes of a subsystem should present similar energetic and damping values in the frequency band of analysis. The second is that a subsystem should present significant energy values so that it influences the energy balance of the system. These two points can be utilized to guide the definition of the subsystems, but they still require experience from the engineer since they do not determine clear partitioning conditions.

3.10 Actran Virtual SEA

The Virtual SEA method applies the concept of the experimental SEA to an energy distributed finite element model and retrieves the SEA matrix of the system. Since the method uses a virtual prototype, its immediate benefits are that the physical model is not required and that the challenges to perform the analysis in a laboratory are eliminated. Also, the constraint of only evaluating bending waves is eliminated since this will depend on the modeling approach of the system [9].

3.10.1 Energetic quantities computation

In the Actran Virtual SEA framework, the subdivision of the system must be defined and stored into a partitioning file. Based on the configuration, the energy distributed model is calculated with the Actran Energy Analysis framework. Once the distribution matrices of the subsystems are known, the Power Injection Method is performed to calculate the frequency and spaced average injected power and energetic values for each subsystem. Therefore, the SEA parameters can be determined based on these energetic values, and afterward, the SEA matrix can be composed and utilized to calculate the response of the structure, given the defined excitation.

It is important to state that the SEA assumptions discussed in section 3.7 should be considered so that the virtual prototype is as close as possible to a "proper-SEA" model.

In the Virtual SEA framework, there are quality indicators that can be requested to verify the validity of the model, such as the modal densities within the range of interest and verifying if the reciprocity conditions are valid.

3.10.2 Boundary conditions

For the Virtual SEA analysis, the injected power will constitute the only boundary condition applied. This excitation must be linear to comply with the SEA assumption. The Actran framework allows direct-injected power, delta correlated loads, distributed loads, or pressure as excitation. However, in this study, "rain-on-the-roof" delta correlated loads will be applied, since this case yields in a simplification of interest, as shown in section 2.4, and the applied load will be proportional to the modal densities.

4. VIRTUAL SEA OF THE SHIP MODEL

As mentioned in section 1.3, a finite element mesh of a RORO vessel has been provided by the ANAST department of the University of Liège. Typically, a Roll-on/roll-off vessel is designed to transport a variety of vehicles such as cars, trucks, trailers, motorcycles, etc. Through the next topics the main assumptions adopted, the pre-processing of the model and the energies results will be detailed.

4.1 Problem Statement

Depending on the ship design purpose, different noise limit criteria might be applied, for instance, if the RORO design is focused on commercial activities, then it is necessary to evaluate the noise levels of the areas where the crew of the ship will be most exposed to. If the vessel will also transport passengers, then within the design there will be common leisure areas and even private cabins for the passengers. In such cases, it is desired to offer as much comfort as possible and the acoustics levels must be verified. Typically, rules that consider passengers will be more demanding than for strictly commercial vessels.

The locations discussed above are located on the upper decks, far from the major noise sources, for instance, the engine room located on the lower decks. However, these are also the regions of the ship that must comply with the most severe noise limits. Thus, in the example with the provided model, the upper decks will be the region of interest of the analysis.

As a reference to verify the sound pressure of the current design, the DNV-GL (2019) rules will be applied. In Part 6 Additional class notations – Chapter 8 Living and working conditions [12], the maximum noise levels for passenger ships and cargo ships are detailed. As there is little information about the utilized model due to confidentiality reasons between the University of Liège and the shipyard, according to the dimensions of the vessel, it will be assumed that there will also be passengers transported and thus the passenger ship values will be used as a reference, as shown in Table 3 whose values are in A-weighted decibels.

In this table, there is also the comfort rating number which will be the classification awarded to the vessel, with the highest standard for a rate 1 and lowest for a rate 3. For example, in a passenger ship, if the complied criteria for the passenger cabins are 1 and 2, the vessel is classified with a rating 2. Nevertheless, in this case, the crew cabins can attend a rate of 3 without affecting the ship rating.

Table 3. Maximum noise levels in dB(A) for passenger ships. Available from
https://rules.dnvgl.com/docs/pdf/DNVGL/RU-SHIP/2019-07/DNVGL-RU-SHIP-Pt6Ch8.pdf
[Accessed 02 June 2, 2020]

Locations	Comfort rating number (crn)		
	1	2	3
Passenger top grade cabins	44	47	50
Passenger cabins, standard	49	52	55
Public spaces	55	58	60
Open deck recreation [1)	65	68	70
1) 5 dB(A) relaxation in sports areas, passage ways and near ventilation inlets and outlets			

Thus, as seen above, the upper deck cabins must attend to a maximum noise value of 55 dB(A) for the lowest rating and 49 dB(A) for the highest, considering only standard cabins.

4.2 Finite Element Mesh Pre-Processing

The known information of the vessel is mostly related to the provided element mesh, the model represents part of the aft part of the vessel. Its main dimensions are 67.2 meters length, 36 meters height, 32.2 meters breadth, and a waterline level of approximately 7 meters. The finite element model contains around 765,000 2D elements representing the hull and some structural elements, and around 170,000 1D elements representing mainly structural elements and connections.

At first glance, it was possible to identify that the finite element mesh has some issues. As exemplified in Figure 14, there are some missing shell elements in different parts of the model and there are 1D elements that are not attached to the 2D nodes.

For a finite element mesh of this size, fixing these small issues can be extremely time-consuming, besides, the modal analysis and the virtual SEA procedure of such a model would not be efficient to test the implementation of a new method which is the aim of this thesis. Therefore, it has been decided to reduce the model to the representation of the midship cross-section, as shown in Figure 15.

With the reduced model, the identified mesh issues could be quickly repaired, and the required computational time is also considerably smaller. Since the provided model is represented by this cross-section over its length, one can assume that the changes performed at the cross-section can be extended to the rest of the vessel.

Nevertheless, it is important to state that the cross-section will represent the behavior of the structure in a *2D-like* analysis since the length of the model is considerably smaller than the other dimensions.
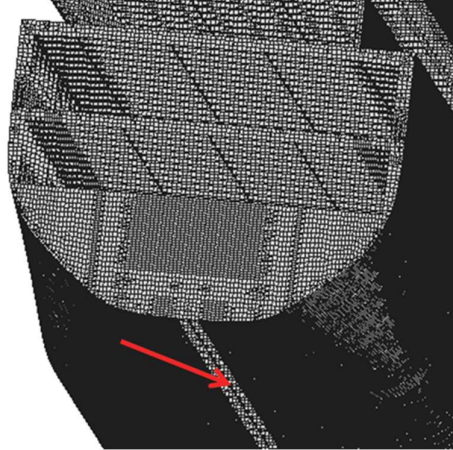
Figure 14. RORO mesh missing shell elements
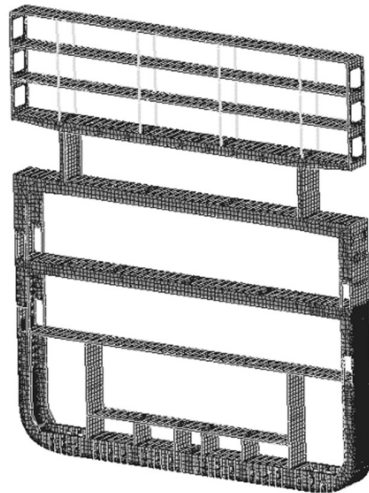
Figure 15. Midship cross-section of the RORO vessel

4.3 Modal Extraction

Before the Virtual SEA, it is required to perform a modal extraction of the model. To do so, the Nastran solver has been utilized. At this point another assumption has been made, the structure is considered to be in "vacuum" which means that the cross-section is not embedded in any fluid, such as the seawater.

Thus, the added mass effect is not considered to perform the modal extraction, as it would increase the complexity of the process. Thus, to some extent, the resonant frequencies will be higher than in practice. Nevertheless, the focus of the study is the development of an efficient method to predict the response of a perturbed SEA model and implement an optimization routine, the most realistic modal extraction, while desirable, is not necessary.

At first, the modes from a range of -1 Hz to 30 Hz have been extracted, the first negative value ensures that all rigid body modes will be captured since no boundary conditions were applied. In Figure *16*, the modal displacement plot of the rigid body modes are shown and, as expected, there are 6 rigid body modes, each of them associated with the 6 degrees of freedom of the model: x, y and z displacements and rotations over the x, y and z-axis.
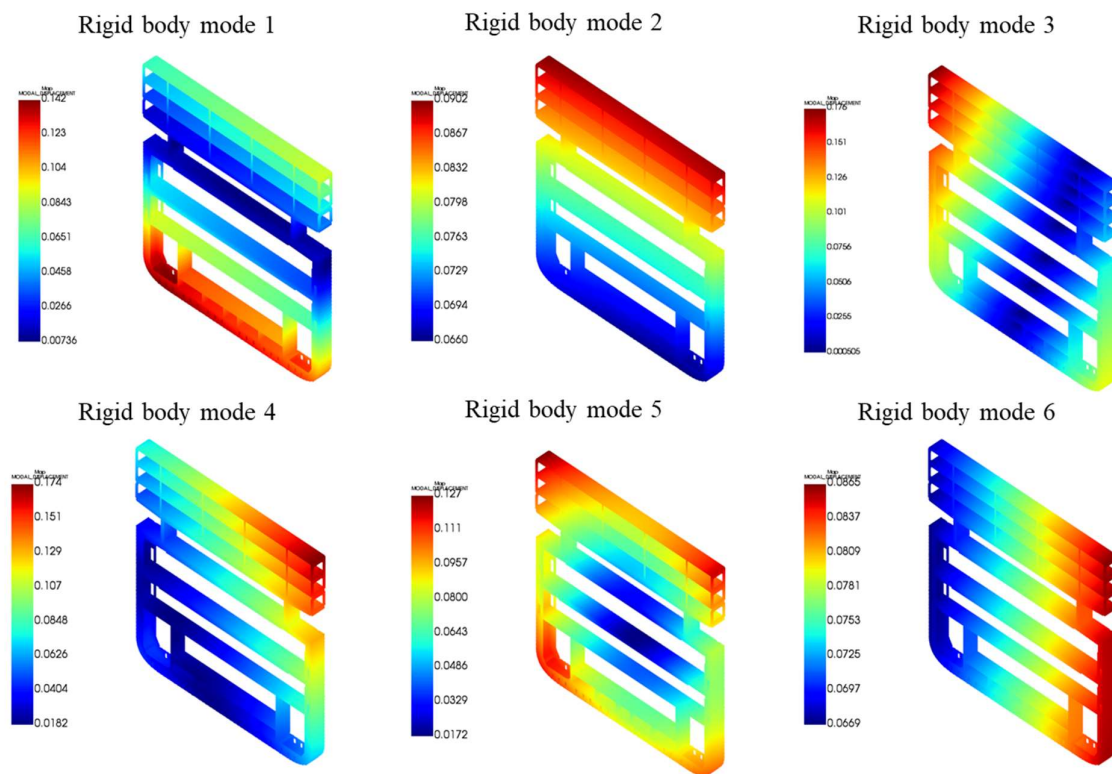
Figure 16. Midship cross-section rigid body modes

However, there are 380 modes in the analyzed frequency range which seems an excessive amount given the small range. This indicates that there might be local modes present in the results. In Table 4, the frequencies of the first 30 resonant modes are shown, and, as expected, these modes are close and confirm the presence of local modes. The modal displacements of the first 4 local modes are plotted and exhibited in Figure 17.

Table 4. Frequencies of the first 30 resonant modes

Mode	Frequency (Hz)	Mode	Frequency (Hz)	Mode	Frequency (Hz)
1	2.13E-05	11	2.860	21	6.980
2	6.78E-06	12	3.950	22	6.980
3	1.89E-05	13	4.380	23	7.020
4	2.08E-05	14	4.800	24	7.030
5	2.53E-05	15	4.920	25	7.170
6	5.47E-05	16	4.990	26	7.270
7	0.977	17	5.550	27	7.270
8	1.460	18	5.720	28	7.390
9	2.290	19	6.650	29	7.530
10	2.720	20	6.960	30	7.540
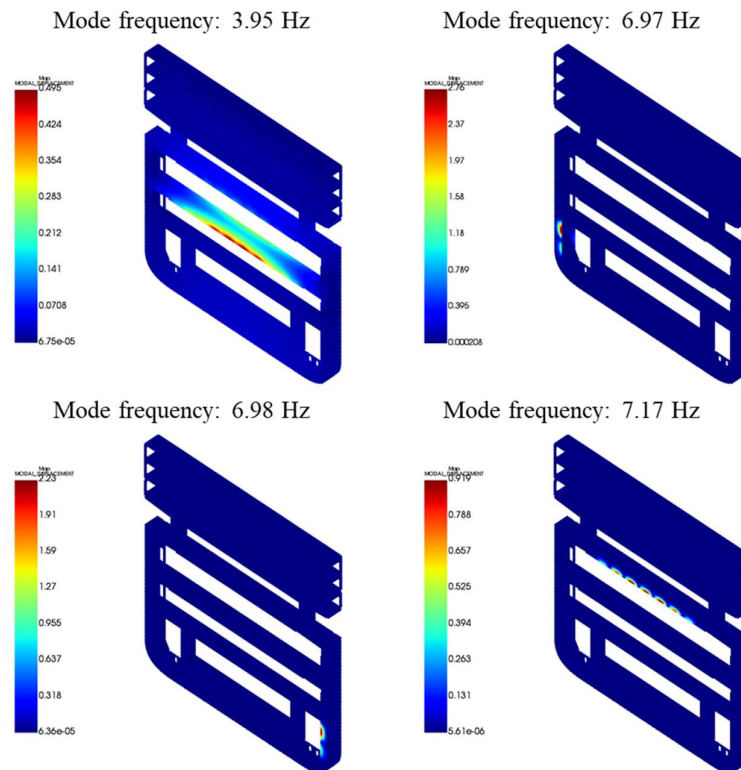
Figure 17. First four local modes of the modal extraction

The presence of these modes shows that the stiffness of the structure is not correctly represented. This might be due to missing elements that were not present in the original mesh or that the stiffening 1D elements are not correctly attached to the shell elements.

Anyhow, the retrieved modal basis has known issues and should not be utilized in a practical application, where the accuracy is essential since great imprecisions will be added to the achieved results.

The next analysis is performed at a frequency range of 700 Hz to 1000 Hz since the SEA method is better suited to high-frequency ranges and the precision is increased for a higher number of modes. Unfortunately, the results of the modal extraction for this frequency range follows the behavior described above.

4.4 Partitioning of the Model

The partitioning of the model is a crucial step of the analysis since it will define whether the SEA assumptions are complied with or not. As seen in section 3.9, there are no well-defined guidelines to divide the model into subsystems. Nevertheless, there are two points to consider in the procedure: the similarity of the modes in energetic terms and the significance of the subsystem. While the first is difficult to correlate to a physical approach, the second is easier, for instance, in the current model it is desired to estimate the noise levels at the deck level. Therefore, the structure can be divided into five subsystems that represent each deck of the cross-section.

Several partitioning configurations have been tested and are shown in Figure 18, where each subsystem is represented by a distinct color. From the left to the right, the simplest to the most complex model is shown.

The first configuration on the left of the figure complies the most with the SEA assumptions, as it will be shown later. All the other configurations violate the assumption of weak coupling between the subsystems and therefore the coupling power proportionality is not guaranteed.
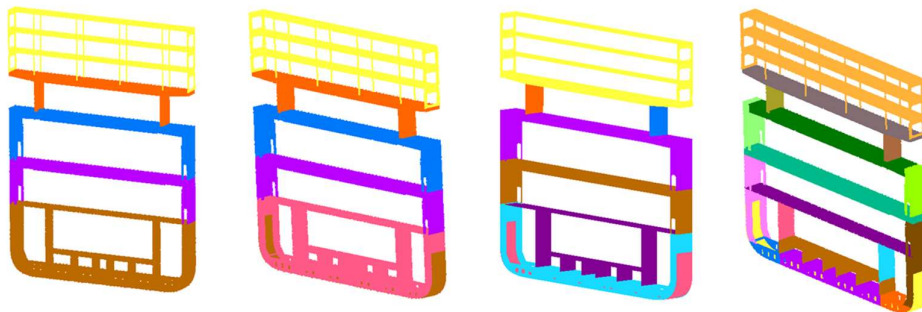
Figure 18. Tested partitioning configurations of the cross-sections

It can be seen that except for the first configuration on the left, the other partitions have a detached part of the bottom and side hull plates. The idea behind the approach was detaching the hull at the waterline height to define an exclusive subsystem to apply an external load. Nevertheless, the coupling within the outer shell of the hull cannot be considered as a weak coupling. In these cases, the Coupling Loss Factors (CLFs) were higher than the Damping Loss Factors (DLFs). As an example, the SEA parameters of the second configuration starting from the left of Figure 18 will be shown.

Figure 19 shows the numbering of the subsystem configuration and Figure 20 plots the magnitude of the SEA parameters for subsystem 5. The dark blue plot represents the DLFs of the subsystem and all the other plots correspond to the CLFs. The DLFs are lower than the CLFs in almost all the frequency range, especially concerning the subsystem 6 where the elements were detached from. The issue is not only seen for this subsystem but the others as well. Thus, these results correspond to a strong coupling which compromises the SEA model.
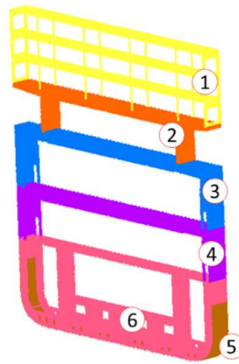
Figure 19. Subsystem numbering of the second partitioning configuration
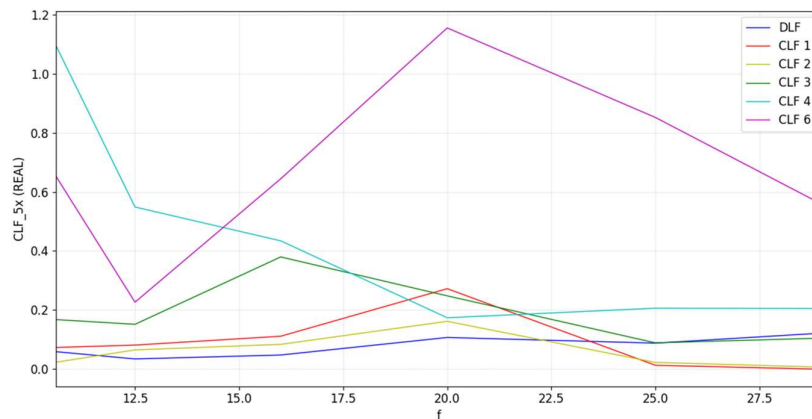
Figure 20. Violation of the weak coupling assumption for a detached hull configuration

4.5 Boundary Condition

Since there is very little information about the model, it is difficult to estimate the excitations acting on the structure. Typically, these sources would be the engines, gearboxes, propellers, HVAC systems, turbulent boundary layers of air and water, exhaust pipes, etc. Even if the types of machinery and operational conditions were known, it is still not an easy task to calculate the excitations magnitudes.

Therefore, as the excitation source, a random delta correlated source is considered, also known as "rain-on-the-roof" excitation, of a magnitude of 10 MPa^2. As it was not possible to detach the outer hull and apply the excitation in an exclusive subsystem, the load will be applied to the subsystem that corresponds to the whole lower deck of the ship.

4.6 SEA Parameters Verification

As mentioned in item 4.3, the analysis will be performed in a frequency range from 700 Hz to 1000 Hz. Thus, the SEA parameters of all the subsystems of the partitioning must be verified within the frequency range of interest. In Figure 21, the numbering of the subsystems is elucidated and in Figure 22, the SEA parameters of the first subsystem are plotted, the verification of the remaining subsystems is on APPENDIX A. From these images, it is seen that all the DLFs are higher than the CLFs, for any subsystem, characterizing a weak coupling between them and attending one of the required conditions of the SEA assumptions.
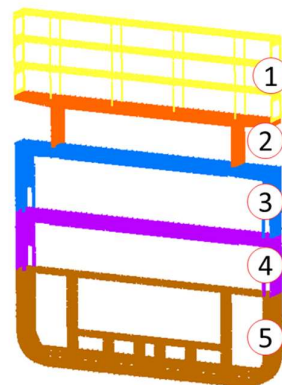
Figure 21. Subsystem numbering of the SEA model
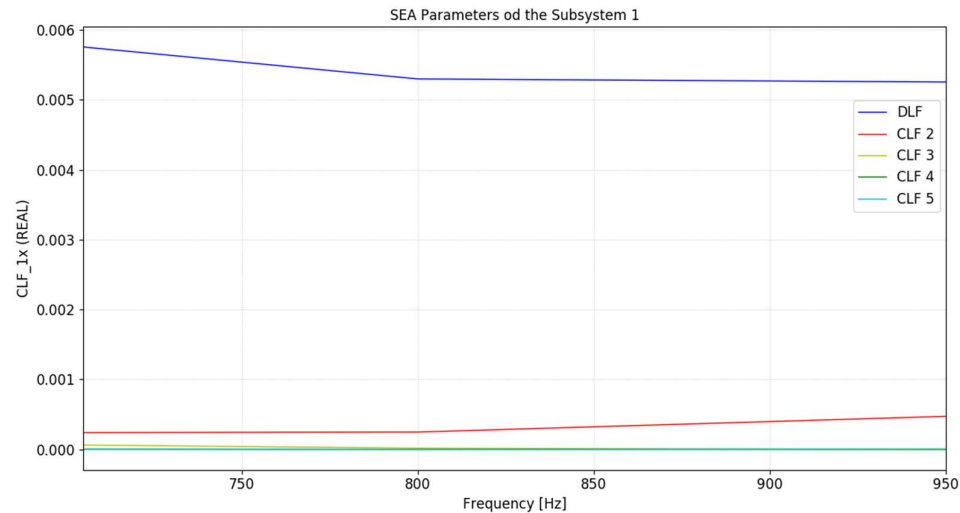
Figure 22. Verification of the subsystem 1 SEA parameters

4.7 Virtual SEA Results

Once the modal extraction is performed, the partitioning is defined and the boundary conditions are set, the virtual SEA can be done. The total energies averaged over a third-octave frequency range from 700 Hz to 1000 Hz are computed using Actran Virtual SEA. The solver divides the requested frequency ranges into three smaller ranges: from 700 Hz to 710 Hz; 710 Hz to 900 Hz and 900 Hz to 1000 Hz. These ranges contain respectively 79, 1730, and 852 modes, a high value due to the strong presence of the local modes. Global damping of 3% is also considered to represent the structural damping which can be understood as the energy dissipated due to the friction between the coupled subsystems.

Since in this example, the noise levels of the upper decks are the main concern, the averaged total energy over a third-octave band of the subsystem 1 is converted to the sound pressure and shown in Figure 23.

The sound pressures are within the rating 3 limit established by DNV-GL rules, however, in the case that the objective of the designer is to classify the ship with a higher rating, an optimization tool is essential to determine the minimum changes required to reduce the energies in the subsystem 1.

The sound pressure of the remaining subsystems is shown in Figure 24 and, as expected, the energies are higher as the subsystems are closer to the source of the input excitations. Thus, the highest values are achieved for the subsystem 5, around 95 dB(A), which are still within the acceptable working range as defined in Figure 5.

However, hearing protection that attenuates at least 25 dB(A) should be provided to the seafarers, in this case. It is important to state that these values have the purpose to illustrate an example of application, since to have an actual correlation to the sound pressure, the air cavities of the compartments must be considered.
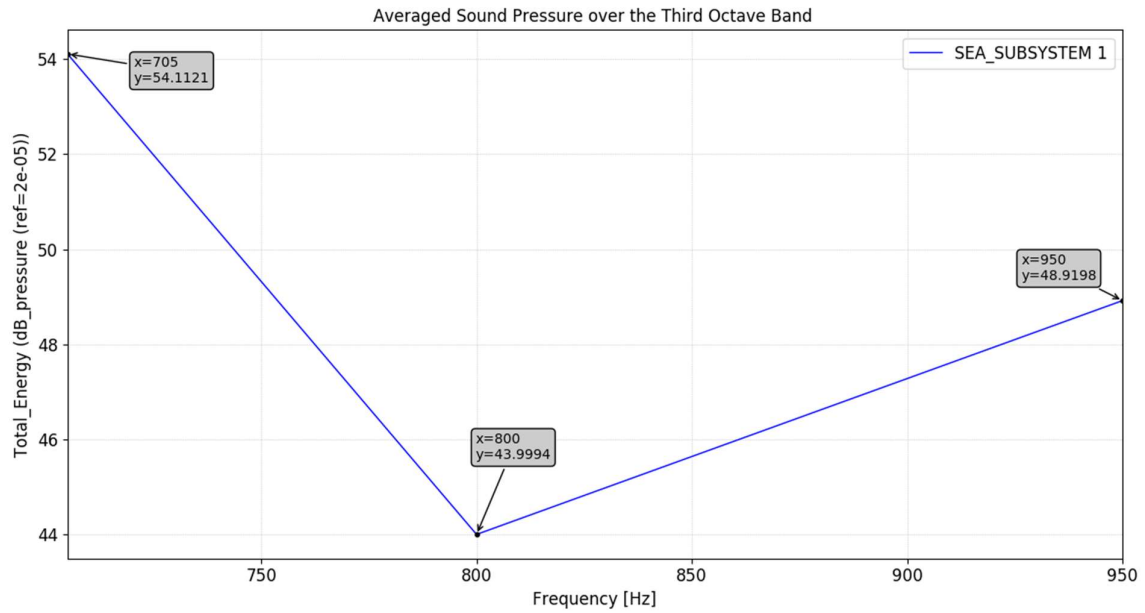
Figure 23. Averaged sound pressure of the subsystem 1
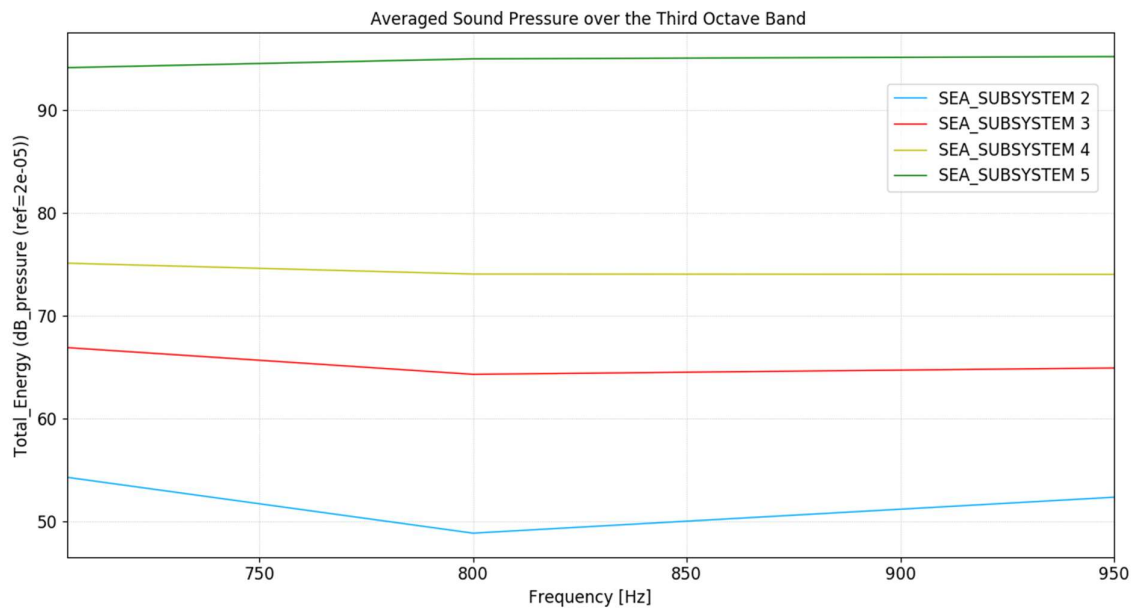
Figure 24. Averaged sound pressure of the remaining subsystems

5. IMPLEMENTATION OF THE APPROXIMATION METHOD

The key point for the success of the thesis is to be able to predict the energy levels of a model with its mechanical properties perturbed, without having to extract the modes and build the distribution matrices of the new configurations. Such computational savings will enable the implementation of an optimization script.

Thus, in this section, different strategies will be discussed that were adopted to attempt to reach these outcomes. All these strategies were implemented in the Actran source code by adding functionalities to the Graphical User Interface (GUI) and the Actran Energy Analysis and Actran Virtual SEA frameworks.

5.1 The Five Plates Model

As seen previously, the cross-section model showed particular issues regarding its modal extraction since it contains many local modes. Therefore, this would impact on the results and reliability of the analysis.

Thus, to reduce the uncertainties of the results, a different model will be utilized for the development of the approximation methods, since the approximated results need to be validated with reliable reference values.

A simpler model that has already been studied and validated by the FFT vibroacoustic team will be considered. This model is composed of five attached steel plates with each representing a distinct subsystem, as shown in Figure 25.

The coupling angles are: between the subsystems 1, 4, and 5, 90°; between the subsystems 1 and 3, 111° and between the subsystems 2 and 5, 147°. The material properties of the plates and their dimensions are shown in Table 5 and Table 6, respectively. In the modal extraction analysis, a finite element mesh of average size 0.01 m is considered and all the edges of the model have their displacements constrained in all directions.

In the Virtual SEA analysis, a global damping of 10% is assumed, and a unitary injected power (W) is applied to subsystem 1. As stated previously, the model has already been validated for frequencies up to 1000 Hz.
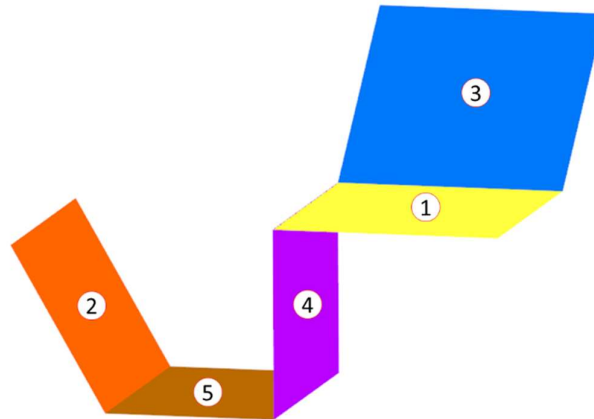
Figure 25. Partition configuration of the five plates model

Table 5. Material properties of the five plates model

Material Properties		Units
Thickness	0.01	m
Young's Modulus	2.10E+11	Pa
Poisson coefficient	0.25	-
Mass density	7820	kg/m^3

Table 6. Plates dimensions of each subsystem

Subsystem ID	Length [m]	Width [m]
1	0.60	0.70
2	0.50	0.70
3	0.60	0.60
4	0.50	0.70
5	0.45	0.70

5.2 Implementation of the SEA Subsystem Properties

Before developing the approximation strategies, a preparatory step is required. Normally in the virtual SEA framework, the stiffness, mass, and damping of each subsystem are not accessible to the user since this information is not necessary.

However, if an optimization routine will be performed, these properties have to be changed in some way. Therefore, it has been decided that these properties will be modified based on perturbation coefficients that express a percentage of change.

For example, if the mass coefficient is 1.05, it indicates that the mass of the specific subsystem will be increased by 5%, if the coefficient is 0.95, then the mass will be reduced by 5%.

Therefore, in the Graphical User Interface (GUI), the SEA subsystem properties were added under the SEA model in the Virtual SEA tree, as can be seen in Figure 26.
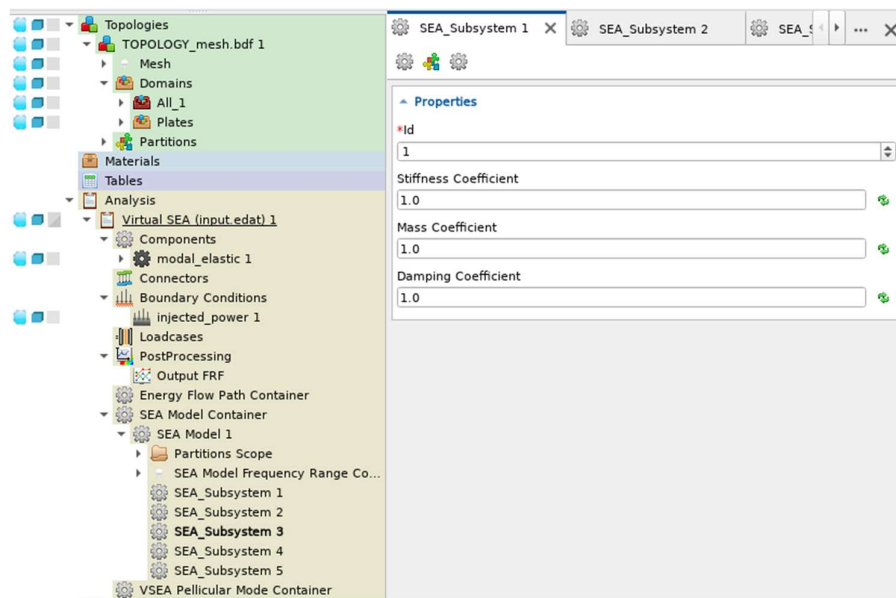
Figure 26. GUI with the subsystem properties nodes

In addition to the implementation of the GUI, the information passed by the user has to be correctly written in and read from the input file of the analysis. Figure 27 shows an example of the input deck of the SEA model.

The information could be added based on previously existing functions. For example, the SEA model contains a node related to extended frequency analysis. Thus, the same functions utilized by this node could be applied to the SEA subsystem nodes. Mostly these are functions from the Python layer of the code which configures the nodes of analysis, the parsing of the information, an Application Program Interface (API) related to the GUI.

```
BEGIN SEA_MODEL 1
  PARTITIONING                1
  THIRD_OCTAVE 300.0 1000.0
  DATABASE ./sea_db.naf
  DIRECTION RANDOM
  SUBSYSTEM_ENERGY KINETIC_ENERGY
  BEGIN SEA_SUBSYSTEM 1
  STIFFNESS_COEFFICIENT 1.0
  MASS_COEFFICIENT 1.0
  DAMPING_COEFFICIENT 1.0
  END SEA_SUBSYSTEM 1
  BEGIN SEA_SUBSYSTEM 2
  STIFFNESS_COEFFICIENT 1.0
  MASS_COEFFICIENT 1.0
  DAMPING_COEFFICIENT 1.0
  END SEA_SUBSYSTEM 2
  BEGIN SEA_SUBSYSTEM 3
  STIFFNESS_COEFFICIENT 1.0
  MASS_COEFFICIENT 1.0
  DAMPING_COEFFICIENT 1.0
  END SEA_SUBSYSTEM 3
  BEGIN SEA_SUBSYSTEM 4
  STIFFNESS_COEFFICIENT 1.0
  MASS_COEFFICIENT 1.0
  DAMPING_COEFFICIENT 1.0
  END SEA_SUBSYSTEM 4
  BEGIN SEA_SUBSYSTEM 5
  STIFFNESS_COEFFICIENT 1.0
  MASS_COEFFICIENT 1.0
  DAMPING_COEFFICIENT 1.0
  END SEA_SUBSYSTEM 5
END SEA_MODEL 1
```

Figure 27. SEA model input deck

5.3 Perturbation of the Energetic Values and DLFs

Once the subsystems' coefficients are available, the strategies to apply the changes to the model can be developed.

The first approximation consisted of perturbating the energetic parameters of each subsystem by multiplying them by the stiffness and mass coefficients while perturbing the DLFs with the damping coefficient. One perturbation is performed at a time, so the effectiveness of each method can be verified.

From a theoretical perspective, this is the easiest and the most straightforward way to perturbate the model since the energetic values are utilized to compose the SEA matrix, as shown in the expressions of the PIM.

Also, from a programming perspective, it is an easy implementation, since these values are already available in some Python functions. Thus, the coefficients just have to be retrieved when necessary to multiply the matrices.

It was expected that the changes in these energetic values would provide an acceptable result. Indeed, the damping perturbation implementation is efficient. Nevertheless, issues were identified concerning the implementation of the mass and stiffness coefficients, which will be discussed further.

5.3.1 Mass and stiffness coefficient implementation

As the SEA parameters are calculated based on the energetic values of each subsystem, if the kinetic and potential energies are multiplied by the mass and stiffness coefficients respectively, the calculated SEA parameters would also be changed. This can be easily understood by the expressions defined in Eq. 2.18 which shows the proportionality of these energies with respect to the properties of the model. However, the mass change should also be applied to the injected power, since under the rain-on-the-roof loading assumption, its values are proportional to the modal mass of the subsystem, as stated in section 2.4.

Therefore, this modification would change the SEA matrix which defines the response of the model, and the final averaged energies should reflect the perturbations.

5.3.1.1 Implementation results

To verify if the implementation is efficient, two analyses were performed: the first increasing the mass of the subsystem 1 by 5% and requesting the averaged kinetic energies; while secondly increasing the stiffness of the subsystem 1 by 5% and requesting the averaged potential energies.

The results of the first analysis are shown in Figure 28. The plot compares the nominal results to the approximated ones for subsystem 1, where the change is applied, and subsystem 5, which is the furthest from the change.

In this plot, it is seen that there is no difference between the two analyses and the curves coincide. The same behavior is seen for all the subsystem energies. Thus, the mass perturbation approach was not effective and it did not achieve the expected result.

The comparison strategy of the second analysis is analogous to the previous plot. Therefore, in Figure 29 it is shown that for subsystem 1, where the change was applied, the potential energies increased, as expected. However, the potential energies of all remaining subsystems are unaltered. This implies that the method can only represent a local change and it is known that if the properties of one subsystem change, modifications of the energy levels will occur all over the model. Therefore, the approach could not achieve the expected outcomes.
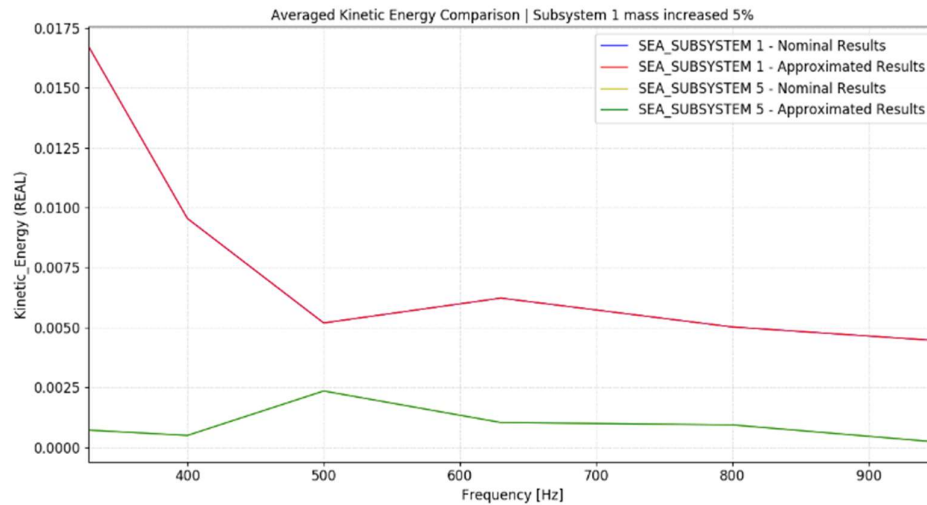
Figure 28. Energies perturbation: comparison of the results for a change in mass
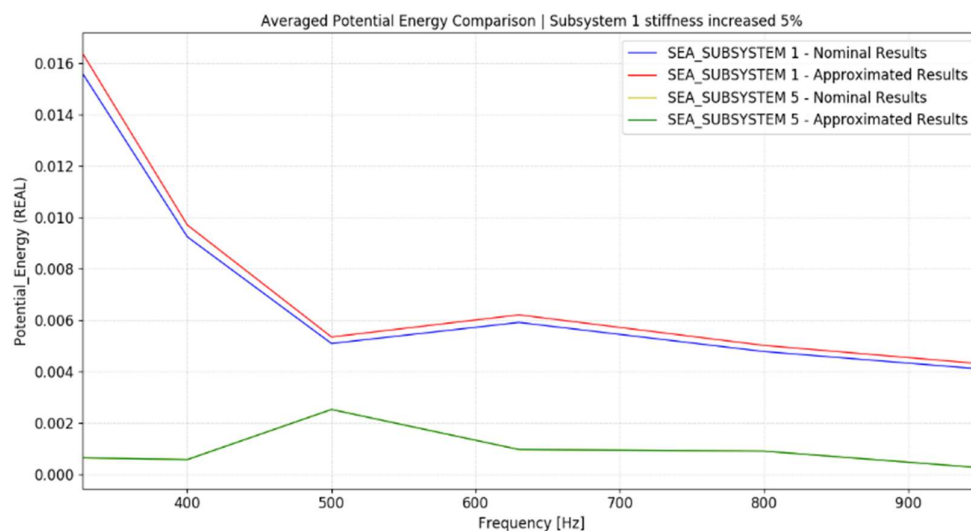
Figure 29. Energies perturbation: comparison of the results for a change in stiffness

5.3.1.2 Identified issues of the implementation

Analyzing the PIM expressions more carefully, the observed behavior in these two approximations attempts can be explained. The changes are made on the energies before the SEA parameters are calculated. Thus, based on Eq. 3.22, the perturbation in the SEA parameters can be expressed as:

$$\Delta\eta_{ij}^{o'} = \omega \frac{(T_{ij}\varepsilon_{m,j} + V_{ij}\varepsilon_{k,j})}{P_j\varepsilon_{m,j}} \tag{5.1}$$

where $\Delta\eta_{ij}^{o'}$ is the perturbation of the parameter, T_{ij} is the kinetic energy, V_{ij} is the potential energy, $\varepsilon_{m,j}$ is the mass perturbation, $\varepsilon_{k,j}$ is the stiffness perturbation and P_j is the injected power.

Thus, the perturbation of the SEA parameter due to the mass change, when only the kinetic energy is considered, equals:

$$\Delta\eta_{ij}^{o'} = \omega \frac{T_{ij}\varepsilon_{m,j}}{P_j\varepsilon_{m,j}} = \omega \frac{T_{ij}}{P_j} \tag{5.2}$$

As the mass coefficient multiplies both the kinetic energy and injected power, the perturbation does not change the energy values since the expression is multiplied and divided by the same coefficient. However, if the total energy is considered, the expression becomes

$$\Delta\eta_{ij}^{o'} = \omega \frac{(T_{ij}\varepsilon_{m,j} + V_{ij})}{P_j\varepsilon_{m,j}} = \omega \left(\frac{T_{ij}}{P_j} + \frac{V_{ij}}{P_j\varepsilon_{m,j}}\right) \tag{5.3}$$

In this case, the total energies are affected since the kinetic power is divided by the perturbed injected power, nevertheless, since the kinetic energy change is not correctly represented, the results are inheritably inaccurate.

For the case where the stiffness is changed, the perturbation equals

$$\Delta\eta_{ij}^{o'} = \omega \frac{V_{ij}\varepsilon_{k,j}}{P_j} \tag{5.4}$$

Differently from the previous case, the change in stiffness is seen in the perturbed subsystem since the injected power is proportional to the mass and not to the stiffness. However, when the PIM power balance is analyzed for the perturbed condition, it yields

$$\begin{bmatrix} P_1 & 0 & \cdots & 0 \\ 0 & P_2 & 0 & 0 \\ \vdots & \vdots & \ddots & \vdots \\ 0 & 0 & 0 & P_r \end{bmatrix} = \omega[\eta^o] \begin{bmatrix} E_{11}(1+\varepsilon_{d1}) & E_{12}(1+\varepsilon_{d1}) & \cdots & E_{1r}(1+\varepsilon_{d1}) \\ E_{21} & E_{22} & \ddots & E_{2r} \\ \vdots & \vdots & & \vdots \\ E_{r1} & E_{r2} & \cdots & E_{rr} \end{bmatrix} \tag{5.5}$$

Thus, the coefficient only changes the energies of the perturbed subsystem and this does not have any effect on all the other subsystems leading to a trivial solution.

5.3.1.3 Conclusions

Although the approach could not achieve the desired results, the process was crucial to better comprehend the method and what could be the alternatives to deal with these perturbations. Fortunately, the computation of the SEA parameters is one of the final steps of the SEA analysis, so there are expressions related to the energy distribution model and the calculation of the energetic levels of the subsystems that can be checked for a possible distinct approach.

5.3.2 Damping coefficient implementation

Differently from the previous approach, the energies are not modified by the damping coefficient. Instead, the damping coefficient will be utilized to perturb the DLFs of the subsystem before the SEA matrix is composed.

The changes can easily be performed by modifying the Python function that composes the SEA matrix. The damping coefficient is retrieved for each subsystem, and the damping term is retrieved from a previous matrix which does not yet correspond to the DLF. Then, this term is multiplied by the damping coefficient and replaced into its origin matrix.

The procedure can be represented in a matrix form, where the first parameters of the main diagonal terms are modified before adding the outgoing CLFs in the matrix composition. If the perturbation is null, then no changes are applied to those parameters.

$$[\eta] = \begin{pmatrix} \eta^o{}_{11}(1+\varepsilon_{d1}) + \sum_{i\neq 1}^{r} \eta^o{}_{1i} & -\eta^o{}_{12} & \cdots & -\eta^o{}_{1r} \\ -\eta^o{}_{21} & \eta^o{}_{22}(1+\varepsilon_{d2}) + \sum_{i\neq 2}^{r} \eta^o{}_{2i} & \ddots & \vdots \\ \vdots & \ddots & \ddots & \vdots \\ -\eta^o{}_{r1} & \cdots & \cdots & \eta^o{}_{rr}(1+\varepsilon_{dr}) + \sum_{i\neq r}^{r} \eta^o{}_{ri} \end{pmatrix} \tag{5.6}$$

5.3.2.1 Implementation results and conclusions

Once more two analyses were performed, this time both evaluating the total averaged energies. The first analysis decreases the damping of subsystem 1 by 5% while the second analysis will increase the damping by the same magnitude.

As previously, the comparison is made between the nominal unchanged values and the approximated results, and also the energies of the subsystem 1 and 5 are compared. The results of the first and second analyses are shown respectively in Figure 30 and Figure 31.

Different from the previous approach, the perturbation of the damping modifies not only the perturbed subsystem energy levels, but it even modifies the energies of the furthest subsystem from the change. The same behavior could also be seen in the results of the remaining subsystems. This global behavior, in this approach, comes from the inversion of the SEA matrix after its composition, thus the change in the DLF of one subsystem will affect all the other SEA parameters.

Also, the results are according to the expectations since reducing the damping, increases the energy levels and the opposite effect is seen when the damping is increased, indicating that the method is consistent.
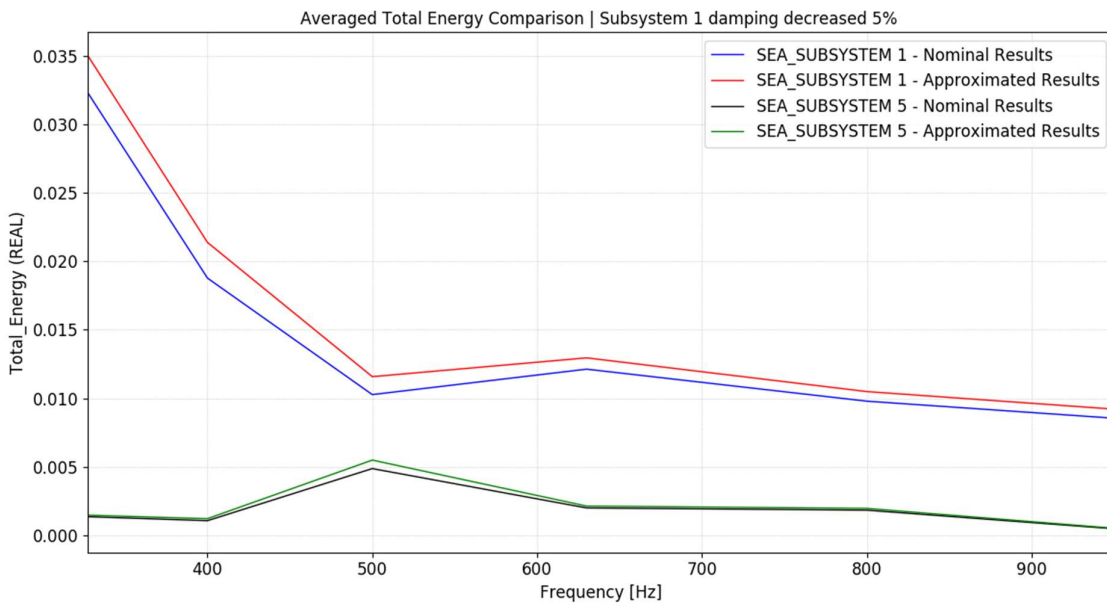
Figure 30. DLFs perturbation: comparison of the results for a decrease in damping
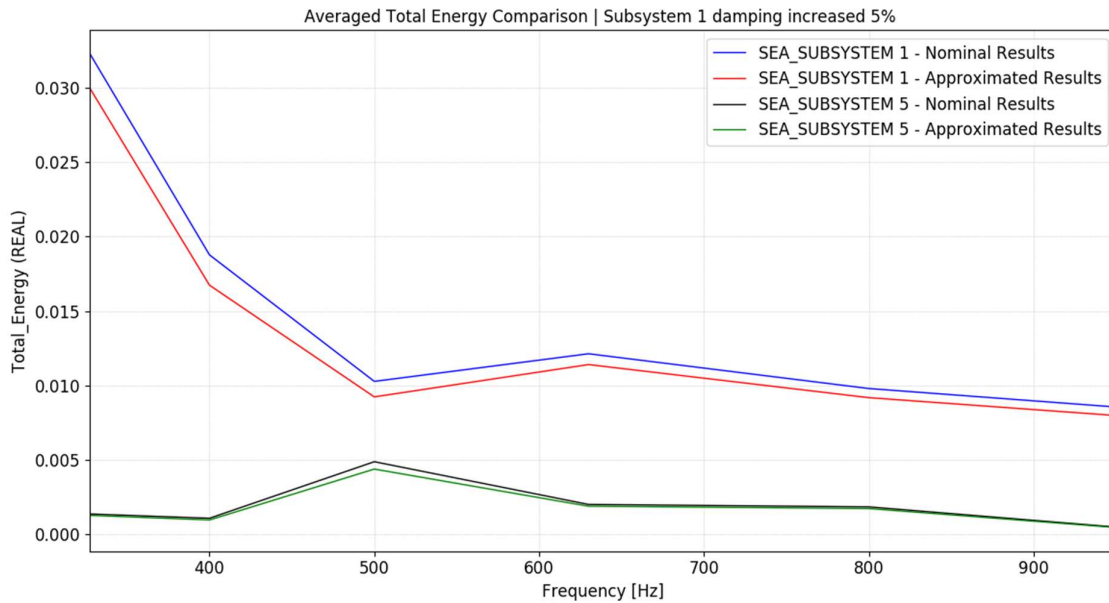
Figure 31. DLFs perturbation: comparison of the results for an increase in damping

5.4 Perturbation of the Modal Densities

Since the perturbation of the subsystems' energetic quantities was not an efficient method to predict the changes in mass and stiffness, the second approach is related to the perturbation of the receptance terms.

In Eq. 2.24, it is seen that these terms, represented by α, are integrated over a frequency range Ω within a broadband B, furthermore, they will multiply the energies of each subsystem which could correctly predict the applied changes in the model.

In the framework of Actran Virtual SEA, these integrals terms are referred to as integrators, and part of the input to calculate them is the modal mass and modal stiffness. These two quantities represent the diagonal of the global mass and stiffness matrices, thus the modal mass will be a vector containing unitary values and the modal stiffness will be a vector containing the square of the eigenfrequencies.

Although the integrators are computed on the C++ layer of the code, the implementation of this approach can still be performed on the Python layer, since the input given is stored in a Python object. Thus, a new function was created to change the vectors and replace them on the object of origin.

5.4.1 Mass and stiffness coefficient implementation

As stated previously, the modal mass and stiffness vectors are the magnitudes of the diagonal of the global mass and stiffness matrices. Therefore, the diagonal of the subsystems' distribution matrices will represent their modal contribution to the system within the frequency range of interest.

As the mass or stiffness is changed, the contributions of each subsystem will also change. Thus, the method consists in calculating the modal contribution φ of each subsystem r by summing the diagonal terms of the distribution matrices and dividing these by the total number of modes N or the total stiffness K, within the frequency range Ω, such that

$$\varphi_{mr,\Omega} = \frac{\sum_{j,\Omega}^N M_{r,jj}}{N_\Omega}, \qquad \varphi_{kr,\Omega} = \frac{\sum_{j,\Omega}^N K_{r,jj}}{K_\Omega} \qquad (5.7)$$

These contributions will always be smaller than unity since each subsystem contains a fraction of the modes. However, the subsystem that contains more modes will have a higher contribution, thus, if a perturbation coefficient is applied to it, it will contribute more to a change of the modal mass or stiffness.

The modal mass and stiffness vectors are the sum of each subsystem contribution. As a consequence, the perturbation applied to it will be a weighted average of all the subsystems' contribution multiplied by their coefficients, within the frequency range Ω, which can be represented by

$$\varepsilon_{m,\Omega} = \sum_{r,\Omega} \varphi_{mr,\Omega} \times \varepsilon_m, \quad \varepsilon_{k,\Omega} = \sum_{r,\Omega} \varphi_{kr,\Omega} \times \varepsilon_k \qquad (5.8)$$

Thus, the global change will be averaged by the modal density of each subsystem and the applied coefficient. In practice, the method changes the eigenfrequencies of the system based on the changes that are applied to each subsystem.

To implement this approach, a Python function has been created and called before the computation of the energetic values of the subsystems. This function retrieves the information about the subsystems' coefficients, the frequency ranges of analysis, and the eigenfrequencies, then it calculates the number of modes within the frequency ranges.

The only information that is more complicated to retrieve is the distribution matrices, since they are only available at the C++ layer, however, through an existing function the matrices can be called a read-only mode which is sufficient for this approach since the distribution matrices will not be modified.

Thus, the procedure loops through the frequency ranges, and within each loop, the contributions of each subsystem are calculated and added to a global coefficient that is applied to the nominal modal mass and stiffness.

5.4.2 Implementation results and conclusions

Once the implementation is done, a series of tests were made by applying coefficients increasing or decreasing the mass and stiffness. In this section, results will only be shown for a simpler analysis, since the method showed similar behavior for both mass and stiffness change.

Therefore, an analysis similar to section 5.4.1 has been performed, where the averaged kinetic energies are requested and the mass of subsystem 1 is changed by 5%.

With this approach, the integrators are being changed and an additional comparison can be done to verify the quality of their prediction. If the nominal model has its material density increased by 5% and the modal analysis and virtual SEA analysis are re-performed, then not only the final averaged energies can be compared but also the integrators. The results from this model will be utilized as a reference to compare with the approximated results.

In this analysis, three different integrals are performed: terms related to the kinetic and dissipated energy and also to the injected power. Since the first two are matrices of order n-modes, their main diagonal has been compared while the latter is a vector. Figure 32, Figure 33 and Figure 34 compare respectively the relative difference between the integrators J of the nominal results, index o, and the integrators of the approximated, index n, and reference results, index p. This difference has been calculated by the expressions

$$\Delta J_{o,p} = \frac{(|J_o| - |J_p|)}{|J_o|}, \qquad \Delta J_{o,n} = \frac{(|J_o| - |J_n|)}{|J_o|} \tag{5.9}$$

Since these terms are frequency-dependent, the results are displayed for the frequency range of the analysis that contains the largest number of modes: 41 modes in the range from 710 Hz to 900 Hz. The orange and blue curves display respectively the reference and approximated values.

It is seen that the trend of the perturbation could be correctly represented with the method, however, for the highest differences, the approximation cannot achieve the same magnitude as the reference values. This can be explained by the averaging of the applied coefficients.

The average considers all the subsystems and since there is no change in any other subsystem of the model, the averaged final coefficient will be lower than the reference solution. In this example, the highest differences from the approximated and reference results reach values around 400%, thus, it is expected that the averaged kinetic energy will also present differences.
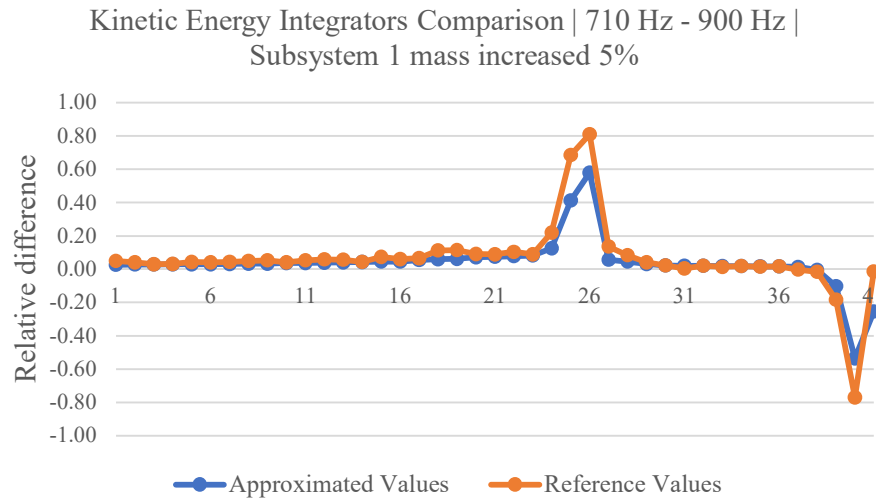
Figure 32. Kinetic energy frequency integrators comparison
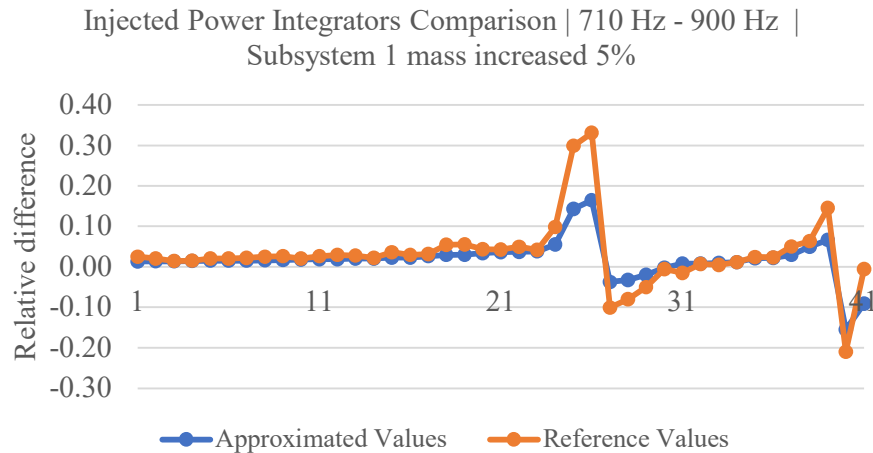
Figure 33. Injected power integrators comparison
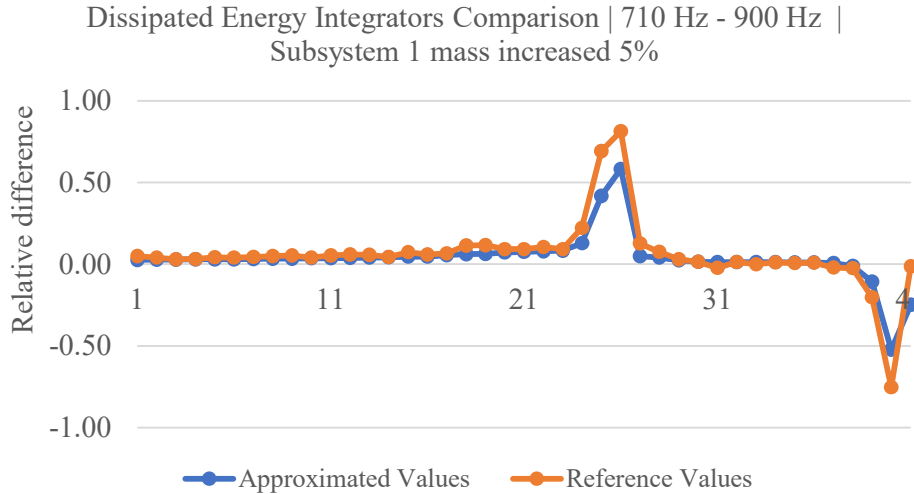
Figure 34. Dissipated power integrators comparison

To verify the issue, Figure 35 plots the averaged kinetic energies of the nominal, reference, and approximated results of the subsystems 1 and 5. It is possible to see that the method predicts a global change and that the mass perturbation in subsystem 1 affects the energy levels of all subsystems. However, the implementation only scales slightly the values of the original curve. The shape of the graphs is essentially the same and different from the validation results.
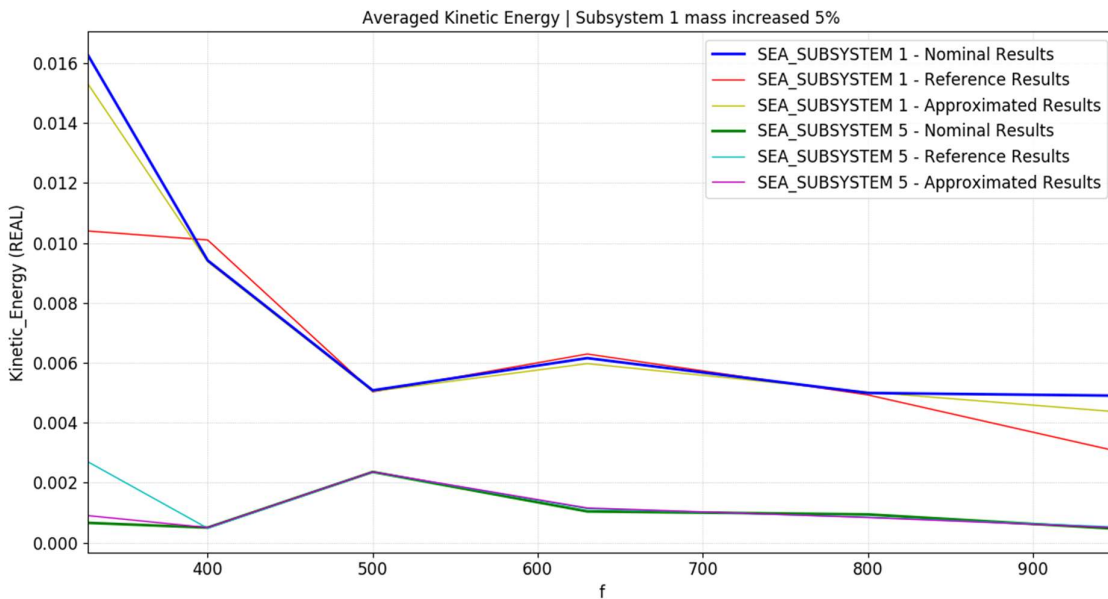
Figure 35. Second implementation energies comparison

Although the approach could not represent accurately the modified structure, it is seen that the integrators perturbation causes a global change. Therefore, if the eigenfrequencies can be predicted with a better method, then the approximation results will more closely approximate the reference results. Another issue that has been observed at this point is that the mass and stiffness distribution matrices of all subsystems change considerably if the properties of one of the subsystems are modified.

5.5 Perturbation of the Distribution Matrices

From the previous method, it became evident that just the modification of the integrators is not sufficient to match the results to the reference.

A preliminary verification identified that the distribution matrices are also changed with the perturbation of the properties of one of the subsystems. As these matrices are a function of the eigenvectors, the change in the modal basis cannot be assumed negligible.

Nevertheless, from a theoretical perspective, it is not straightforward to understand how the perturbations will modify these matrices, thus, the change that is applied will present a certain similarity with the previous approach.

However, differently from the last two approaches, the distribution matrices cannot be changed from the Python layer as they are available in read-only mode.

Therefore, the adopted strategy was to calculate the changes within the Python layer and by adapting the function that retrieves these matrices, a vector will be passed from Python to C++. Then, the matrices can be modified and stored in the buffer. This will prevent the changes from being overwritten later in the code. Like the previous approach, the modifications of the distribution matrices must be done before the calculation of the energetic values of the subsystems.

5.5.1 Mass coefficient implementation

From the results of the previous method, it was seen that the perturbation of the mass or stiffness of a subsystem produced results with similar behavior, as the approach was essentially the same for both.

Therefore, in this implementation, only the expressions related to the mass change have been developed and analyzed, if the achieved results would have been satisfactory, then the solution would have been extended to the change in stiffness by replacing the mass terms with the stiffness.

In the previous approach, the terms that were changed are frequency-dependent and had to be computed for each frequency range. The distribution matrices are not frequency-dependent; thus, the averaging will be defined by the division of each diagonal term by the trace of the mass distribution matrix of the subsystem r

$$\varepsilon'_{m,r} = \left(\frac{M_{jj.r}}{\sum M_{jj,r}}\right) \times \varepsilon_{m,r} \tag{5.10}$$

Therefore, the modes that have a higher contribution within the subsystem will have their change enhanced by this averaging. Nevertheless, as this change is calculated based on the diagonal of the matrix, the modification can only be applied to its diagonal terms, such as

$$M'_{jj,r} = M_{jj.r} \times (1 + \varepsilon'_{m,r}) \tag{5.11}$$

It is worth reinforcing that if the coefficient is applied to all the terms of the mass distribution matrix equally, the results will be the same as in the first approach when the kinetic energy was multiplied by the coefficient directly.

In the second approach, the reference model showed that all the distribution matrices should be modified if a perturbation is applied for one of the subsystems. Thus, as an attempt to reproduce this behavior, the mass distribution matrices of the unchanged subsystems are also perturbated.

As seen in Eq. 5.12, the average of the subsystem s is calculated and multiplied by the coefficient applied to the subsystem r, but with an opposite sign, divided by the number of unchanged subsystems n_s:

$$\varepsilon'_{m,s} = \left(\frac{M_{jj.s}}{\sum M_{jj,s}}\right) \times \frac{-\varepsilon_{m,r}}{n_s} \tag{5.12}$$

And the modified mass matrix diagonal is

$$M'_{jj,s} = M_{jj.s} \times (1 + \varepsilon'_{m,s}) \tag{5.13}$$

To implement this approach, a function has been developed to calculate the second term of Eq. 5.13, these vectors are then stored according to the specific subsystem.

The modified values of the mass matrix diagonal could be computed directly and stored as vectors, however, in Actran the framework, the energetic values are calculated from the distribution matrices at the patch level. As a subsystem is composed of one or multiple patches, their diagonal is not the same as for the subsystems.

Thus, before calculating the energies for each patch, these coefficients are retrieved and passed to the C++ layer and then the modification of their distribution matrix can be performed.

5.5.2 Implementation results and conclusions

Several tests have been performed with this approach for different configurations. However, the results achieved are very similar to the previous approach, as shown in Figure 35, and will not be replicated in this item.

Even if the previous approach is utilized in combination with the distribution matrix manipulation, the energy levels are just slightly scaled and there is no significant improvement or worsening of the results.

The distribution matrices of the subsystems are densely populated and from a reference model, it is seen that its values change all over the matrix. Therefore, the changes in the diagonal of the mass distribution matrix are not sufficient to predict correctly its perturbation.

5.6 Eigenproblem Perturbation

At this stage of the development, although the previous implementations could not achieve the desired outcome, each step was essential to better comprehend the problem.

It was seen that the perturbation of the integrators will simulate the shift of the eigenfrequencies when the mechanical properties of the systems are modified.

In addition, the distribution matrices are a function of the mass and stiffness magnitudes but also the eigenvectors of the system. Therefore, if it is possible to predict accurately the perturbation of the eigenfrequencies and eigenvectors, the changes can be extended to define the perturbed distribution matrices and the frequency integrals.

One of the advantages from a programming perspective, as it will be seen, is that the derived expressions will modify the integrators, distribution matrices, and the modal forces. Thus, as the first two components were already modified in the previous implementations, the functions could be adapted for this approach.

5.6.1 Mass and stiffness coefficient implementation

As the full derivation of the eigenproblem perturbation is extensive, the development will elucidate the final perturbation expressions.

The modal extraction of a system solves the eigenproblem equation defined as

$$\lambda_i = \phi_i^T (K - \lambda_i M)\phi_i \tag{5.14}$$

where λ are the eigenfrequencies squared ω^2.

When the mass or stiffness of a system is changed, it is evident that its natural frequencies will not remain unaltered. If the change is small enough and remains in the linearity range, and neglecting higher-order terms, the partial differential equation of the expression (Eq. 5.15) can be approximated by its finite differences with Nelson's approach [13].

$$\partial \lambda_i = \phi_i^T (\partial K - \lambda_i \partial M)\phi_i \tag{5.15}$$

Then, there are two possible scenarios yielding different expressions. The scenarios are: if the mass is changed then the derivations are made concerning the mass M; if the stiffness is changed, then the derivations are made concerning the stiffness K. It will also be assumed that the changes made in a local subsystem will reflect the global changes in the structure.

Based on these assumptions, the expression of the perturbation of the eigenfrequencies can be defined by a mass change, index m, and a stiffness change, index k, of the subsystem r, such as

$$\Delta \lambda_m = -\lambda_0 \, \varepsilon_{m,r} \widetilde{M}'_{r,ii}; \qquad \Delta \lambda_k = \varepsilon_{k,r} \widetilde{K}_{r,ii} \tag{5.16}$$

where $\widetilde{M}$ and $\widetilde{K}$ are the mass and stiffness distribution matrices, respectively.

The expressions of the eigenvectors perturbations will be

$$\Delta \phi_m = -\frac{1}{2}\widetilde{M}_{r,ii}\varepsilon_{m,r}\phi_i + \sum_{i \neq j} \frac{\lambda_{0i}}{\lambda_{0j} - \lambda_{0i}} \, \widetilde{M}_{r,ij}\varepsilon_{m,r}\phi_j$$

$$and$$

$$\Delta \phi_k = \sum_{i \neq j} \frac{-1}{\lambda_{0j} - \lambda_{0i}} \widetilde{K}_{r,ij}\varepsilon_{k,r}\phi_i \tag{5.17}$$

For a simplification of the perturbation expressions of the distribution matrices, from these two last expressions, two matrices have been defined that express the perturbations due to the mass or stiffness change. They are defined by the scaling of the nominal distribution matrices:

$$C_{m,r} = -\frac{1}{2}\widetilde{M}_{r,ii} + \frac{\lambda_{0i}}{\lambda_{0j} - \lambda_{0i}}\widetilde{M}_{r,ij}; \qquad C_{k,r} = \frac{-1}{\lambda_{0j} - \lambda_{0i}}\widetilde{K}_{r,ij} \tag{5.18}$$

As these matrices will be utilized in all the following expressions, computational savings are achieved if they are calculated and stored once. Then expressions for the perturbation of the mass and stiffness distributions are defined by

$$\Delta \widetilde{M}_{m,r} = \varepsilon_{m,r} \widetilde{M}_r C_{m,r} + \varepsilon_{m,r} C_{m,r}^T \widetilde{M}_r + \varepsilon_{m,r} \widetilde{M}_r$$
$$\Delta \widetilde{M}_{k,r} = \varepsilon_{k,r} \widetilde{M}_r C_{k,r} + \varepsilon_{k,r} C_{k,r}^T \widetilde{M}_r + 0 \tag{5.19}$$

$$\Delta \widetilde{K}_{m,r} = \varepsilon_{m,r} \widetilde{K}_r C_{m,r} + \varepsilon_{m,r} C_{m,r}^T \widetilde{K}_r + 0$$
$$\Delta \widetilde{K}_{k,r} = \varepsilon_{k,r} \widetilde{K}_r C_{k,r} + \varepsilon_{k,r} C_{k,r}^T \widetilde{K}_r + \varepsilon_{k,r} \widetilde{K}_r \tag{5.20}$$

For the case study, where the delta correlated forces are proportional to the mass distribution matrix, the perturbation of the random modal forces will follow similar expressions as the mass distribution perturbation, such as

$$\Delta \widetilde{F}_{m,r} = \varepsilon_{m,r} \widetilde{F}_r C_{m,r} + \varepsilon_{m,r} C_{m,r}^T \widetilde{F}_r + \varepsilon_{m,r} \widetilde{F}_r$$
$$\Delta \widetilde{F}_{k,r} = \varepsilon_{k,r} \widetilde{F}_r C_{k,r} + \varepsilon_{k,r} C_{k,r}^T \widetilde{F}_r + 0 \tag{5.21}$$

These expressions define the changes of the perturbed subsystem. However, it is also necessary to define the expressions that the change will induce in the remaining subsystems. This has been represented by multiplying the subsystems' s matrices with the C_m and C_k matrices and ε coefficients of the perturbed subsystem r. Thus, the equations will be

$$\Delta \widetilde{M}_{m,s} = \varepsilon_{m,r} \widetilde{M}_s C_{m,r} + \varepsilon_{m,r} C_{m,r}^T \widetilde{M}_s$$
$$\Delta \widetilde{M}_{k,s} = \varepsilon_{k,r} \widetilde{M}_s C_{k,r} + \varepsilon_{k,r} C_{k,r}^T \widetilde{M}_s \tag{5.22}$$

$$\Delta \widetilde{K}_{m,s} = \varepsilon_{m,r} \widetilde{K}_s C_{m,r} + \varepsilon_{m,r} C_{m,r}^T \widetilde{K}_s$$
$$\Delta \widetilde{K}_{k,s} = \varepsilon_{k,r} \widetilde{K}_s C_{k,r} + \varepsilon_{k,r} C_{k,r}^T \widetilde{K}_s \tag{5.23}$$

$$\Delta \widetilde{F}_{m,s} = \varepsilon_{m,r} \widetilde{F}_s C_{m,r} + \varepsilon_{m,r} C_{m,r}^T \widetilde{F}_s + 0$$
$$\Delta \widetilde{F}_{k,s} = \varepsilon_{k,r} \widetilde{F}_s C_{k,r} + \varepsilon_{k,r} C_{k,r}^T \widetilde{F}_s + 0 \tag{5.24}$$

All the shown equations could be efficiently implemented in Actran's source code. The perturbations are calculated in three different steps. At first, the perturbation of the mass and stiffness distribution matrices are calculated, storing the modified distribution matrices and the C_m and C_k matrices within their respective subsystem object

In the second step, the perturbation of the modal forces is done by modifying an existing function and it is done before the application of the PIM. As their perturbation follows the mass perturbation, the C_m and C_k matrices are retrieved from each subsystem's object.

The third step is the perturbation of the eigenfrequencies, the expressions are also implemented in an existing function before the integrators are computed. There is also another important step in the implementation. As stated previously, the energetic calculation is performed at the patch level, thus each patch must be matched to its parent subsystem, and then the modified matrices are retrieved. However, this is only possible if the subsystems are

represented by a single patch which is the case of the five plates model. If there are multiple patches within the subsystem, the implementation will fail since the subsystem's distribution matrices will be distinct from the patches. Nevertheless, the possibility to calculate the energetic values at the subsystem level is being developed by FFT's vibroacoustic team, which will allow for the implementation of the method for more complex models. Since this alternative is in its validation stage, it could not be utilized in this project.

The described approach differs from the two last implementation attempts since it is relatively more complex and because it defines unique perturbation expressions for the changes in mass and stiffness.

As there are a series of values that are predicted, such as the distribution matrices, eigenfrequencies, and modal forces, it is necessary to verify whether the results are accurate. Therefore, two scenarios are considered: the first is an analysis of the averaged kinetic energy when the mass of subsystem 1 is increased by 1% and the second is an analysis of the averaged potential energy when the stiffness of subsystem 1 is increased by 1%.

As a reference to compare the results for each modification, the analysis will be re-performed by changing, respectively, the material density and Young's modulus by the same magnitude.

5.6.2 Eigenfrequencies comparison

The first compared prediction is the eigenfrequency perturbation. Since the applied coefficients are relatively small, the change will be compared by the percentage of change between the approximated and the reference values λ' to the nominal eigenfrequencies λ, as expressed by

$$\Delta\lambda(\%) = \frac{\lambda' - \lambda}{\lambda} \times 100 \tag{5.25}$$

It is expected from such a small perturbation that the magnitudes of change for a mass and stiffness increase will be similar but with opposite signs. Also, as the mass is increased the eigenfrequencies should be lowered and increased if the stiffness is increased.

Therefore, within a frequency range of 100 Hz to 700 Hz, the changes of the eigenfrequencies are shown in Figure 36 and Figure 37, respectively for the increased mass and stiffness. For both scenarios, the eigenfrequencies could be approximated to values close to the

reference results and the curves almost overlap to its full extent. It is also seen that the changes have a similar magnitude with opposite signs corresponding to the expectations.

The good accuracy achieved with the eigenfrequency approximation will affect directly the integrators' magnitudes. Thus, differently from the results of the second approach, the integrators' perturbation could be estimated with good precision.
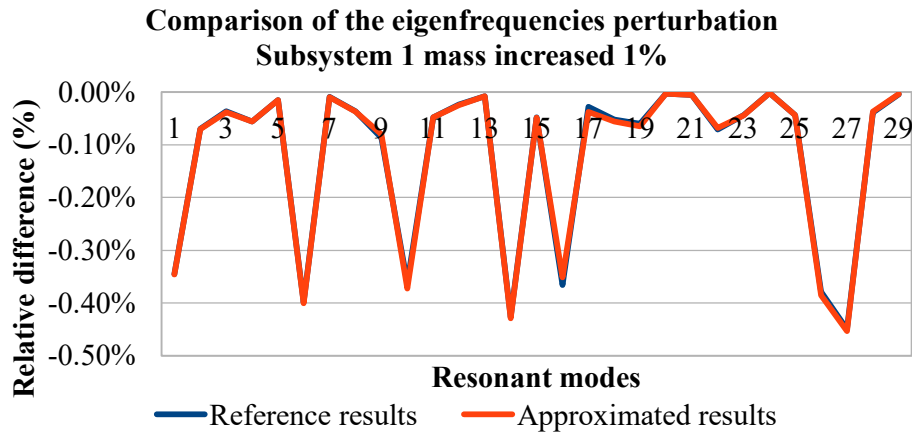

Figure 36. Comparison of the eigenfrequencies perturbation for the mass change
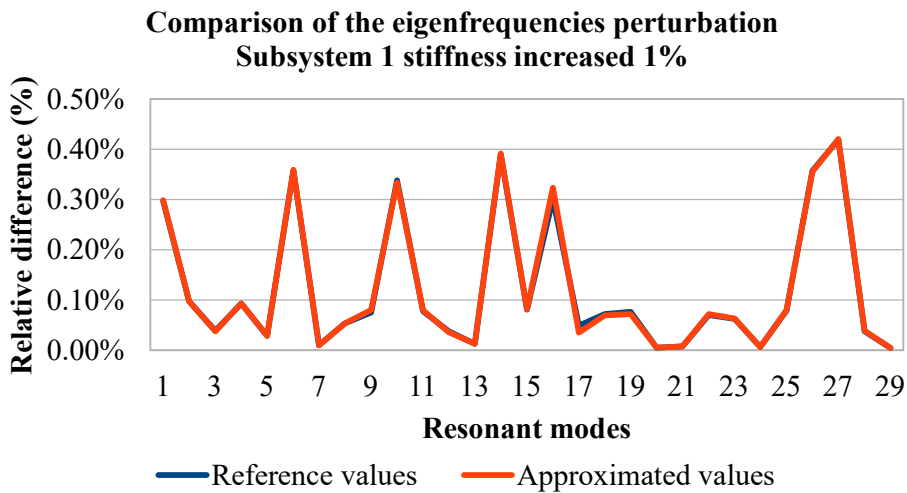
Figure 37. Comparison of the eigenfrequencies perturbation for the stiffness change

5.6.3 Mass distribution matrices comparison

Furthermore, the approximation of the distribution matrices must be compared to the matrices of the nominal and reference model. However, such a comparison might not be straightforward since these are square matrices of order n-modes.

One way to compare the similarity between them is by calculating their distance, the smaller the distance the more similar they will be. Thus, the distance expressed in the matrix comparison will be defined by

$$d_{ab} = \sqrt{\sum_j^n \sum_i^n (|a_{ij}| - |b_{ij}|)^2} \qquad (5.26)$$

In the third implementation approach, only the main diagonal of the mass distribution matrix had been modified, and the method was insufficient to represent the change. In this approach, the perturbation of the mass matrices is made in all of its terms.

Table 7 and Table 8 show the comparison respectively for the cases where the mass and stiffness of subsystem 1 is increased by 1%. In both tables, the distances between the nominal and the approximated matrices, the nominal and reference matrices, and the reference and approximated matrix are calculated for all the subsystems.

Table 7. Mass distribution matrices distance for a mass increase

Mass distribution matrix Mass increased	Distance Nominal to Approximated	Distance Nominal to Reference	Distance Reference to Approximated
Subsystem 1	0.171	0.142	0.037
Subsystem 2	0.147	0.112	0.038
Subsystem 3	0.086	0.084	0.010
Subsystem 4	0.143	0.123	0.027
Subsystem 5	0.107	0.094	0.017

Table 8. Mass distribution matrices distance for a stiffness increase

Mass distribution matrix Stiffness increased	Distance Nominal to Approximated	Distance Nominal to Reference	Distance Reference to Approximated
Subsystem 1	0.155	0.192	0.047
Subsystem 2	0.132	0.179	0.052
Subsystem 3	0.085	0.089	0.011
Subsystem 4	0.114	0.110	0.013
Subsystem 5	0.085	0.100	0.020

Due to the small change applied to the model, the distance between the matrices are low in magnitude, however, it is evident that the distances of the approximated and reference model to the nominal matrices are much higher than the distance between themselves.

Thus, this last distance shown in the third column represents a fraction of the other two columns. This shows that the approximated matrices are much closer to the reference values than the nominal. Therefore, it can be concluded that the prediction of the mass distribution matrices of any subsystem is accurate enough for either the changes in mass or stiffness.

5.6.4 Stiffness distribution matrices comparison

A similar comparison can be made concerning the stiffness distribution matrices. In Table 9 and Table 10, the results are shown as it was done for the mass distribution matrices.

It is seen that once more the distances between the approximated and reference matrices are the smallest, confirming a good accuracy of the method.

Table 9. Stiffness distribution matrices distance for a mass increase

Stiffness distribution matrix Mass increased	Distance Nominal to Approximated [x10^5]	Distance Nominal to Reference [x10^5]	Distance Reference to Approximated [x10^5]
Subsystem 1	17.750	14.076	5.520
Subsystem 2	17.539	13.285	4.547
Subsystem 3	6.370	5.671	1.130
Subsystem 4	16.988	14.538	3.173
Subsystem 5	11.987	10.300	2.069

Table 10. Stiffness distribution matrices distance for a stiffness increase

Stiffness distribution matrix Stiffness increased	Distance Nominal to Approximated [x10^5]	Distance Nominal to Reference [x10^5]	Distance Reference to Approximated [x10^5]
Subsystem 1	15.815	20.258	5.302
Subsystem 2	15.437	21.099	6.176
Subsystem 3	5.525	6.364	1.263
Subsystem 4	12.677	12.799	2.237
Subsystem 5	8.444	10.550	2.468

However, one of these distances is of particular interest. In Table 9, the distance between the reference and approximation of subsystem 1 is proportionally higher than the other values. For instance, this distance is 5.52, higher than the distance in Table 10, 5.302. For the same case, the distance between the reference to the nominal will be 14.076 and 20.258, respectively.

Therefore, the perturbation for a mass change is smaller than for the stiffness change. However, it seems that errors in this prediction are higher than expected.

To verify the hypothesis, the difference between the terms of the reference and approximation are plotted. The differences will be defined as

$$\Delta \mathrm{ab}_{ij} = \left\| |a_{ij}| - |b_{ij}| \right\| \tag{5.27}$$

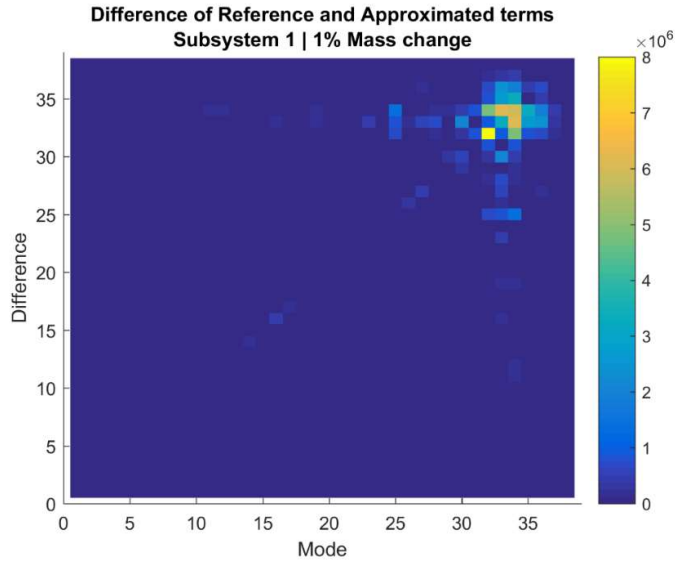and the plots are shown in Figure 38 and Figure 39.

Figure 38. Colormap of the difference between the reference and approximation stiffness distribution matrices for a mass increase
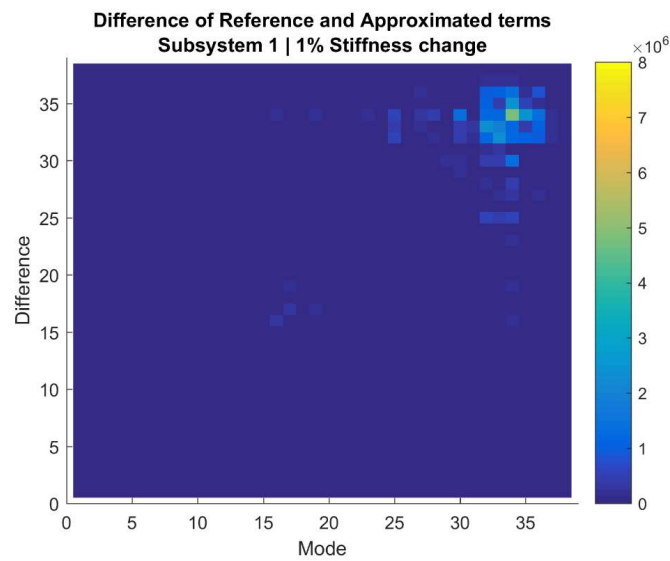

Figure 39. Colormap of the difference between the reference and approximation stiffness distribution matrices for a stiffness increase

As suspected, there are more terms and with higher magnitudes in the mass change approximation than in the stiffness, especially as the modes increase. Since the applied coefficients are low in magnitude, it is expected that the accuracy of both approximations would achieve congruent results.

However, this cannot be seen in this case and there is an increased imprecision associated with the prediction of the stiffness distribution matrix for a mass change and exclusively on the perturbated subsystem. Other tests have been performed, and this behavior has been consistent in different scenarios.

Thus, the inaccuracy of the prediction of this matrix will affect considerably the final averaged potential energy. Until deeper investigations are performed to understand the reason for this specific ill-conditioned behavior, evaluations of the potential energies are not recommended with the approximation method.

Nevertheless, the sound-related analysis is strongly correlated to the kinetic energy while the potential energy is more related to the stresses and strain. Since the method can be utilized to predict accurately the kinetic energies, it can still be efficiently implemented.

5.6.5 Random modal forces matrices comparison

Regarding the random modal force perturbation, since it follows the same expressions of the mass change, the results are expected to be the same as shown previously.

In Table 11 and Table 12, the assumption can be confirmed since all the calculated distances of these matrices are the same as the predictions for the mass distribution matrices, and the same good accuracy is achieved.

Table 11. Random modal force matrices distance for a mass increase

Random modal force matrix Mass increased	Distance Nominal to Approximated	Distance Nominal to Reference	Distance Reference to Approximated
Subsystem 1	0.171	0.142	0.037
Subsystem 2	0.147	0.112	0.038
Subsystem 3	0.086	0.084	0.010
Subsystem 4	0.143	0.123	0.027
Subsystem 5	0.107	0.094	0.017

Table 12. Random modal force matrices distance for a stiffness increase

Random modal force matrix Stiffness increased	Distance Nominal to Approximated	Distance Nominal to Reference	Distance Reference to Approximated
Subsystem 1	0.155	0.192	0.047
Subsystem 2	0.132	0.179	0.052
Subsystem 3	0.085	0.089	0.011
Subsystem 4	0.114	0.110	0.013
Subsystem 5	0.085	0.100	0.020

5.6.6 SEA matrices and averaged kinetic energies comparison

All the previous approximations mainly affect the energetic values and the injected power of PIM equations. Therefore, if the approximations are good enough, the predicted SEA matrix will also be closer to the reference SEA matrix. Thus, the distance of the SEA matrix was analyzed for each frequency range between 100 Hz and 700 Hz.

In Table 13 and Table 14, these distances are shown for the mass and stiffness increase of subsystem 1, respectively. As the previous predictions were closer to the reference model, the behavior can be seen once more in the SEA matrix prediction.

By the last frequency range, the distances concerning the nominal matrix are approximating the distance between reference and approximation matrices which might be correlated to imprecisions of the method for higher frequencies and very small changes in the properties.

Table 13. SEA matrices distance for a mass increase

SEA matrix Mass increased	Distance Nominal to Approximated	Distance Nominal to Reference	Distance Reference to Approximated
SEA matrix [112 Hz to 140 Hz]	0.237	0.224	0.013
SEA matrix [140 Hz to 180 Hz]	0.329	0.321	0.008
SEA matrix [180 Hz to 224 Hz]	0.076	0.073	0.003
SEA matrix [224 Hz to 280 Hz]	0.013	0.012	0.001
SEA matrix [280 Hz to 355 Hz]	0.006	0.006	0.001
SEA matrix [355 Hz to 450 Hz]	0.011	0.010	0.001
SEA matrix [450 Hz to 560 Hz]	0.007	0.007	0.002
SEA matrix [560 Hz to 710 Hz]	0.008	0.006	0.003

Table 14. SEA matrices distance for a stiffness increase

SEA matrix Stiffness increased	Distance Nominal to Approximated	Distance Nominal to Reference	Distance Reference to Approximated
SEA matrix [112 Hz to 140 Hz]	0.029	0.030	0.006
SEA matrix [140 Hz to 180 Hz]	0.636	0.710	0.085
SEA matrix [180 Hz to 224 Hz]	0.120	0.153	0.033
SEA matrix [224 Hz to 280 Hz]	0.012	0.016	0.005
SEA matrix [280 Hz to 355 Hz]	0.007	0.007	0.003
SEA matrix [355 Hz to 450 Hz]	0.006	0.009	0.005
SEA matrix [450 Hz to 560 Hz]	0.009	0.008	0.003
SEA matrix [560 Hz to 710 Hz]	0.006	0.008	0.004

Interestingly, the magnitudes of the changes seem to decrease as the frequency is increased. For higher-frequency ranges, the model behavior is closer to a "proper-SEA". As a consequence, the properties change in the subsystem will be local and should affect less the remaining subsystems.

Figure 40 and Figure 41 show the differences between the reference and nominal SEA matrices, for a mass change, in the ranges of 140 Hz to 180 Hz, and 560 Hz to 710 Hz, respectively. It can be seen that the order of magnitude of the first plot is considerably higher and there are many non-related terms to subsystem 1. While for the second, these terms are less present and with reduced magnitude. In this case, the highest changes are located in the first column and row since they are related to the change applied to subsystem 1.
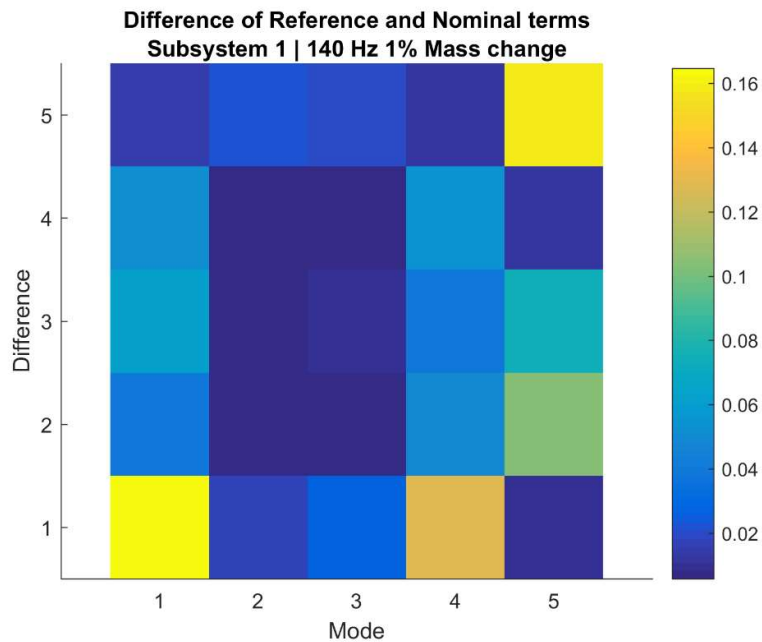
Figure 40. Comparison of the SEA matrix difference 140 Hz to 180 Hz
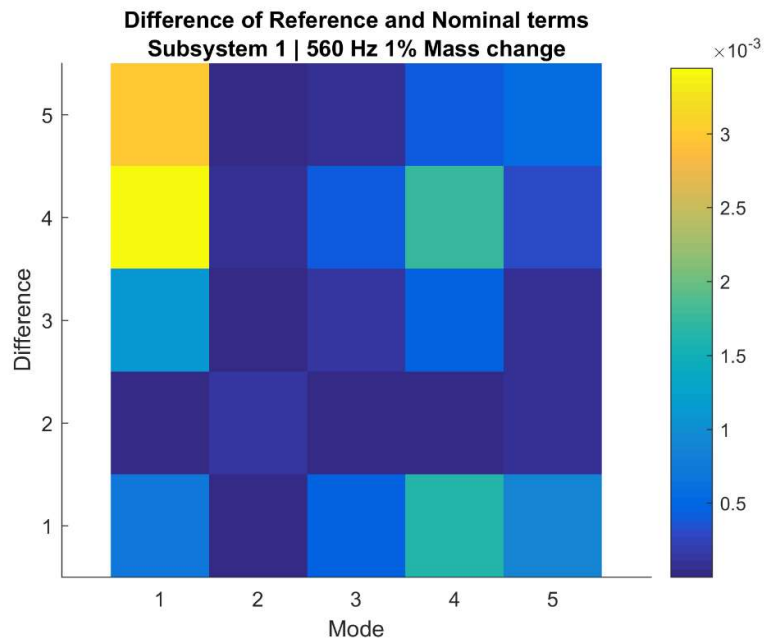
Figure 41. Comparison of the SEA matrix difference 560 Hz to 710 Hz

The plot of the averaged kinetic and potential energies (Figure 42 and Figure 43) show that the approximation results are very close to the reference values and that their curves are a nearly perfect overlap over the frequency range.
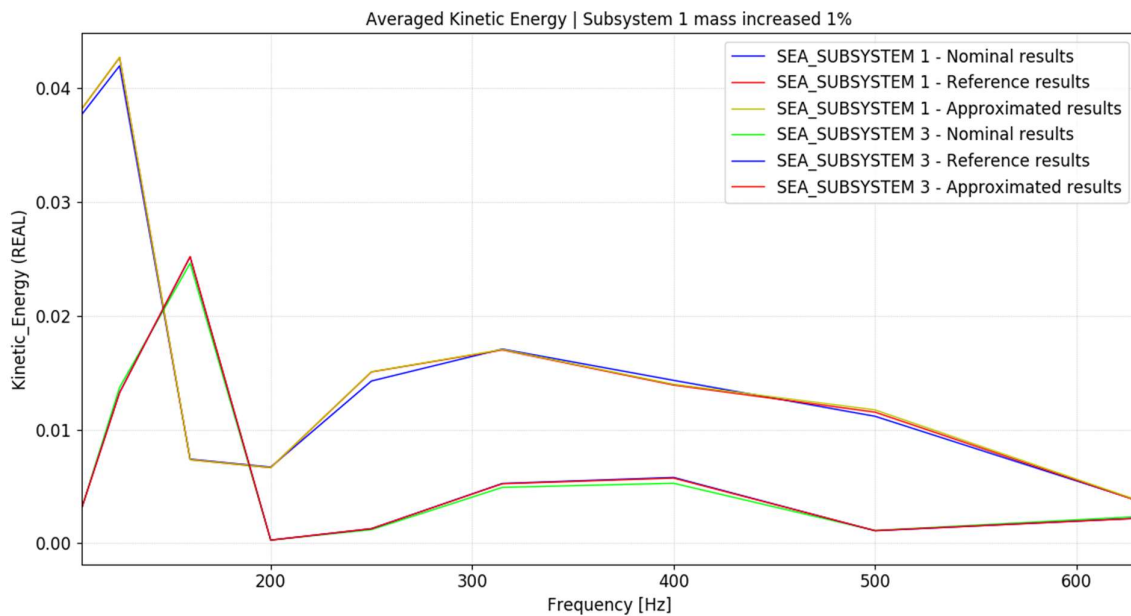
Figure 42. Averaged kinetic energy comparison for a mass increase in subsystem 1
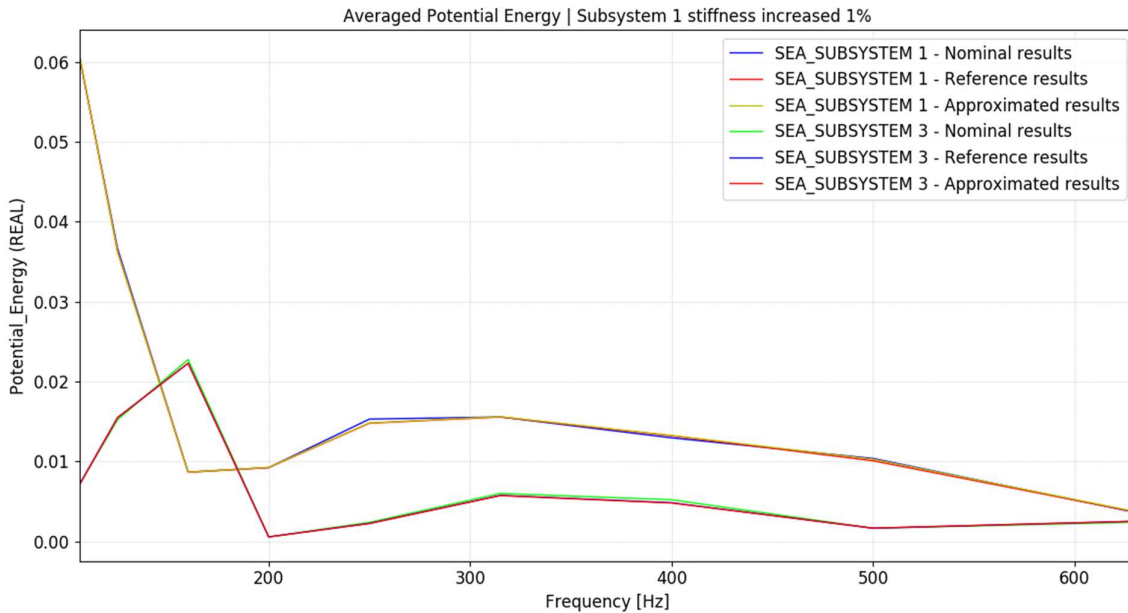
Figure 43. Averaged potential energy comparison for a stiffness increase in subsystem 1

5.6.7 Validity of the approximation

Some concerns must be considered when utilizing the approximation implemented in this topic. Part of the assumption of the derivations of the perturbation of the eigenproblem equation is that the changes will be small enough so that the perturbations remain linear, the number of modes is the same and that there are no shifted modes. If any of these assumptions is not respected, the accuracy of the method will be lowered.

As an example, the mass of the subsystem 1 is increased by 5% and the averaged kinetic energies are measured. As shown in Figure 44, the approximation can represent the trend of the change accurately for the lower frequencies, but as the frequencies increase, the results are distant from the reference.

In this specific example of the five plates model, acceptable results could be achieved by changing the properties ±3%.

Also, as discussed previously, due to imprecisions related to the prediction of the stiffness distribution matrix when the subsystem has its mass perturbed, the potential energy has a less reliable result and this issue must be investigated further.
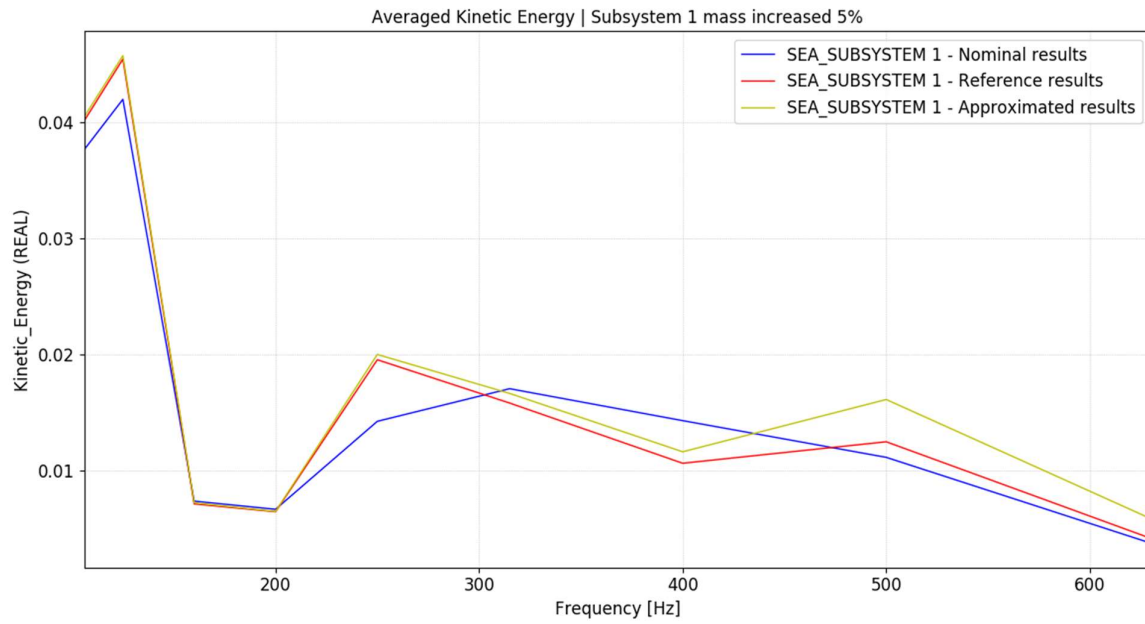
Figure 44. Averaged kinetic energy comparison for a mass increase of 5% in subsystem 1

6. DEVELOPMENT OF THE OPTIMIZATION TOOL

As shown previously, the last approximation approach could achieve satisfactory results for the prediction of the averaged kinetic energies with a perturbated model. Thus, as one of the goals of the study, an optimization script has been developed and applied to the five plates model.

The results of the implementation are compared with a reference model, where its properties have been changed and the modal extraction and the distribution matrices are recomputed.

Furthermore, an optimization script has been developed in a scenario where the approximation method is not available, thus, for each iteration, the modal extraction, and the distribution matrices must be computed.

Then, the computational cost of the two optimization approaches is compared along with the achieved final energy results.

6.1 Optimization Script and Strategies

From the results shown in section 5.6, it is possible to see that subsystem 1 has an energy peak at a frequency of 125 Hz. The plot of the averaged kinetic energy is shown as the equivalent sound pressure of the plate in Figure 45.

Figure 45. Averaged sound pressure of subsystem 1

It might be the case in a practical application that the design must satisfy a criterion of a sound pressure lower than 80 dB(A), thus the designer could launch an optimization requesting the minimization of the specific energy.

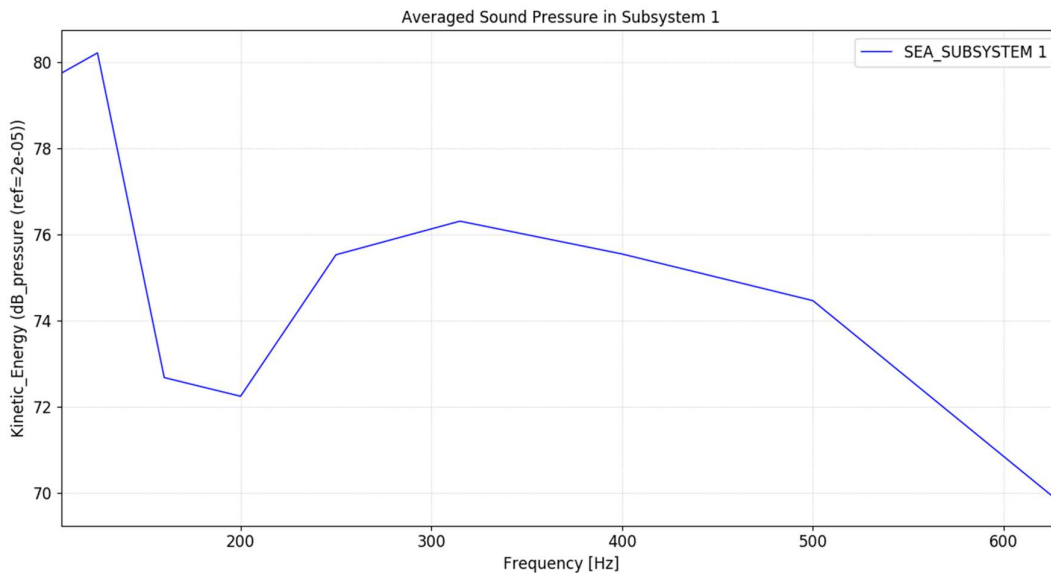To solve such problems, several approaches can be done. For instance, if the perturbation coefficients are bounded within a range of maximum increase and minimum decrease, and the minimization of the energy is requested, it is expected that the energies will be greatly reduced if the boundaries are large enough. However, the approach might not be realistic since it might be required the addition or removal of mass or stiffness from the design, implying great design changes.

A more interesting approach, and the one adopted in the following items, is minimizing the change of the model to achieve the desired energy reduction. Besides the boundaries of the coefficients, the change of the coefficients has been restricted so their sum equals the norm of an unchanged model, in this case, 5. Thus, the properties of the subsystems are redistributed along the model achieving a sensibility of the necessary changes.

At this point, the damping coefficients could also be implemented in the optimization script. However, since the configuration would be harder to validate with a reference model, only the changes in mass and stiffness will be considered.

With the subsystem properties available to the Actran's source code, it was possible to develop an optimization script with the NLOPT package which is adapted to the solvers available in Actran. The algorithm utilized was the Constrained Optimization by Linear Approximations (COBYLA). Its framework set linear approximation of the objective function and constraints and optimizes these values for each iteration of the process. It also allows the implementation of nonlinear inequality constraints that might be useful according to the needs of the designer. For example, in the case of the five plates model, the objective function can be the minimization of the energy level for a specific frequency. An inequality constraint might be added to the energies of the surrounding frequencies, enforcing that they will be lower than the original value and not necessarily minimized.

Two optimization approaches will be done: the first utilizes the implemented approximation method, and the second is solved conventionally by extracting the modes in each of the optimization iterations.

As identified in section 5.6, as the coefficients are increased and the changes start to become nonlinear, the method loses its accuracy gradually. To prevent this issue from happening, the optimization routine is divided into two steps.

At first, the script launches the optimization in order to reduce the kinetic energy at the frequency of 125 Hz by 10%. The boundaries for the perturbation coefficients are defined as ±3%, and their sum is limited to 5 each so that the change is also minimized. After the optimization is finished, the coefficients are retrieved, the modal extraction is re-performed and the distribution matrices are deleted. Then, another script is called to reduce the energy to a target of 20% and with the same configurations as before.

At last, an optional step is performed to increase the accuracy of the results. The coefficients are retrieved and the modal extraction is performed, then the same optimization script as the second step is launched. This procedure is enabled due to the low computational cost of each iteration. Also, because the initial step will be closer to the optimum configuration, the convergence is quickly achieved.

The second optimization script, which is here regarded as a reference, is simpler. For each iteration, the modal extraction is performed based on the properties change and the distribution matrices are rebuilt. The energy reduction target is the same, 20% at 125 Hz, the boundaries of the coefficients are increased to ±5% and their sum must also be 5.

6.2 Optimization of the Five Plates Model with the Approximated Method

Due to the restriction on the coefficient boundaries, the amount of energy that can be reduced within one optimization script is limited. Thus, as a method to extend the use of the approximation method, the modal extraction is re-performed when a defined energy level is reached. For instance, in this example, after the target energy was reduced by 10% at 125 Hz, the modal extraction was done and the optimization followed until a 20% reduction was achieved. The last modal extraction is an optional step to ensure the precision of the final results.

Figure 46 shows the evaluation of the objective function of the whole procedure. It is seen that around 400 iterations were required to achieve the convergence of the results. Not only must the results comply with the energy target but also with the sum of the coefficients.

Therefore, the number of iterations might be reduced if fewer constraints are applied to the procedure. However, the whole process, including the modal extractions, was done in 14 minutes and 32 seconds, a relatively low cost considering that the optimization was reset three times.
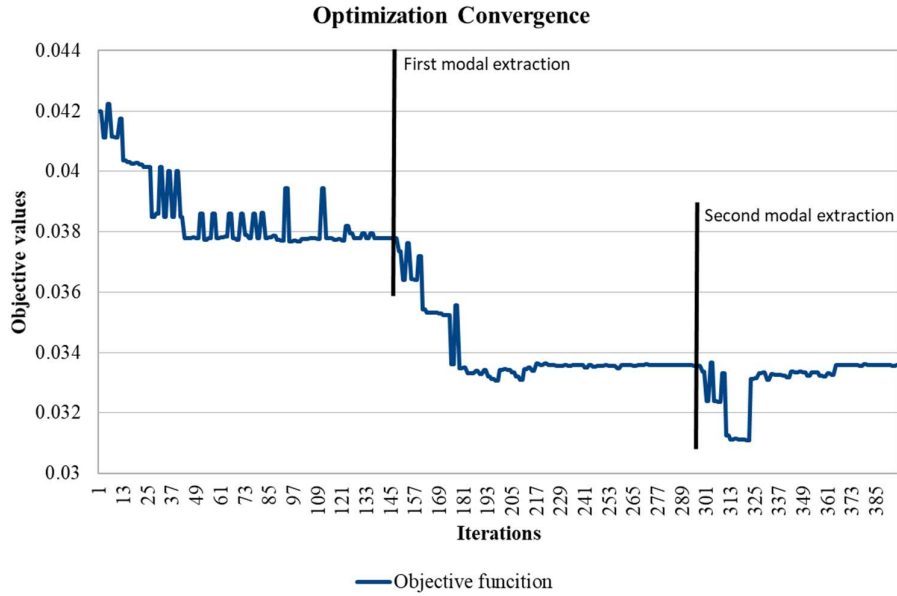
Figure 46. The convergence of the objective function of the first optimization loop

A comparison is done similarly as in the previous topics. The averaged kinetic energy was plotted for the nominal, approximated, and reference results, so the values can be compared.

The plot in Figure 47 shows that the peak at 125 Hz could be efficiently reduced to below the 80 dB(A). Also, as a consequence of the additional modal extraction at the end of the optimization, the optimization result matches the reference values through the frequency range of analysis with a very small difference. Thus, the provided results are reliable and the optimization approach, efficient. The final reduction coefficients will be shown further in the comparison of this optimization with the second approach.
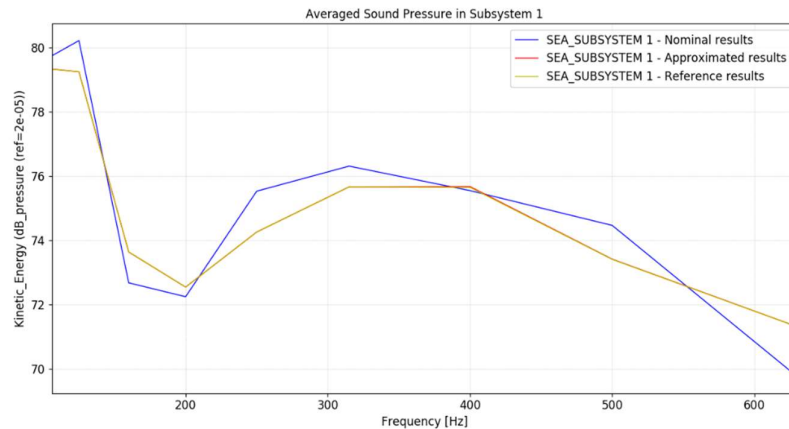
Figure 47. Comparison of the averaged kinetic energy optimization result

6.3 Optimization of the Five Plates Model with a Conventional Approach

In the case where the approximation method is not available, the only option to perform this analysis is by changing the mechanical properties of the model at each iteration and re-extracting the modes and building the distribution matrices of the model.

For the same tolerances, objective functions and constraints as the previous optimization, the number of iterations of this method is diminished by half, as shown in Figure 48. The convergence is not achieved promptly since the sum of the coefficients is constrained so that there is no increase of mass or stiffness in the results.

Even though the optimization required half of the iterations, the total time of analysis was 1 hour 53 minutes and 20 seconds, 7.8 times higher than the optimization with the approximation method. Other optimization tests were performed with different objectives and frequency ranges, and the approximation was always more efficient than this approach.

The energy results and the final optimized coefficients will be compared and discussed in the next topic.

Figure 48. The convergence of the objective function for the second optimization loop

6.4 Comparison of the Optimization Results
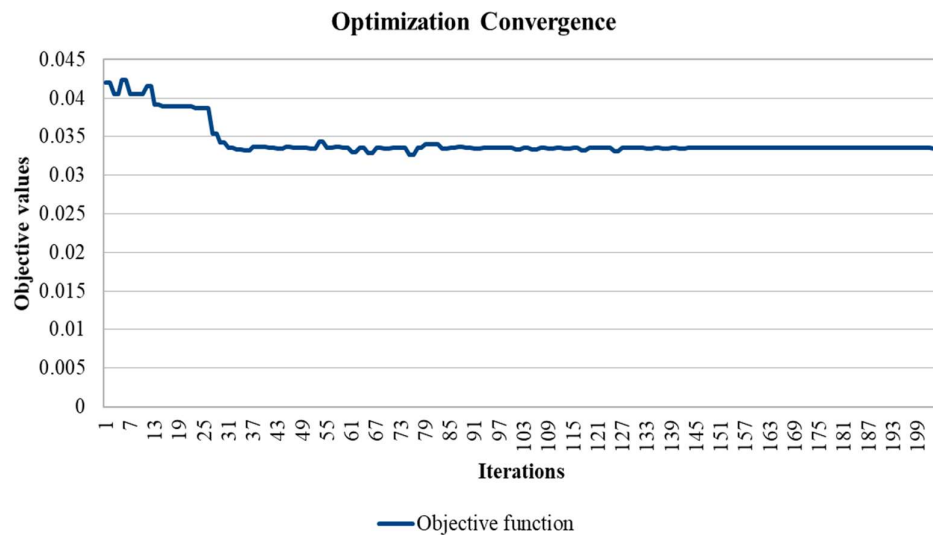
The sum of the perturbation coefficients was imposed to remain the same, as if no changes are applied to the model. It is seen in Table 15 that the optimization with the approximation method has this constraint slightly violated since each time the modal extraction is performed, another optimization script is launched, and therefore, the final coefficients will be the combination of all the three steps. Nevertheless, the exceeded value is negligible since it represents an increase of 0.1% on the mass and stiffness.

The achieved coefficients of both optimizations are very close in some subsystems, such as the case for subsystem 1 and 3. However, for subsystems 2, 4, and 5 there are some mismatches with the sensitivities of the coefficients.

As the two approaches are very distinct and the optimization algorithms are only able to achieve local minima and not global, the results would hardly be identical. These differences can be interpreted as different design approaches that would lead to the main objective, which is reducing the peak energy level of subsystem 1.

Table 15. Comparison of the achieved coefficients for each design approach

Coefficients comparison	Approximated Stiffness coefficient	Reference Stiffness coefficient	Approximated Mass coefficient	Reference Mass coefficient
Subsystem 1	1.033	1.049	0.957	0.960
Subsystem 2	0.987	0.970	1.007	0.980
Subsystem 3	0.975	0.986	1.022	1.024
Subsystem 4	1.019	0.999	1.010	1.002
Subsystem 5	0.987	0.996	1.004	1.034
Σ	5.001	5.000	5.001	5.000

In Figure 49, the reference, first approximated optimization and the second reference optimization results are shown.

For the frequency of 125 Hz, both methods complied with the energy constraint and the reduction is 20%. However, since the modification of the nominal model is not identical for both approaches, there are energy differences. Between 200 Hz and 400 Hz, the approximated optimization results are slightly higher than the reference optimization, and the opposite is seen between 500 Hz to 700 Hz.

Thus, the two approaches achieved similar design configurations, respecting the minimization of the change of the properties of the model and providing the knowledge of the sensibility of the mass and stiffness change to the system behavior. However, the approximation approach is able to achieve the optimum configuration for a negligible cost, around 7 times smaller than for the conventional approach.
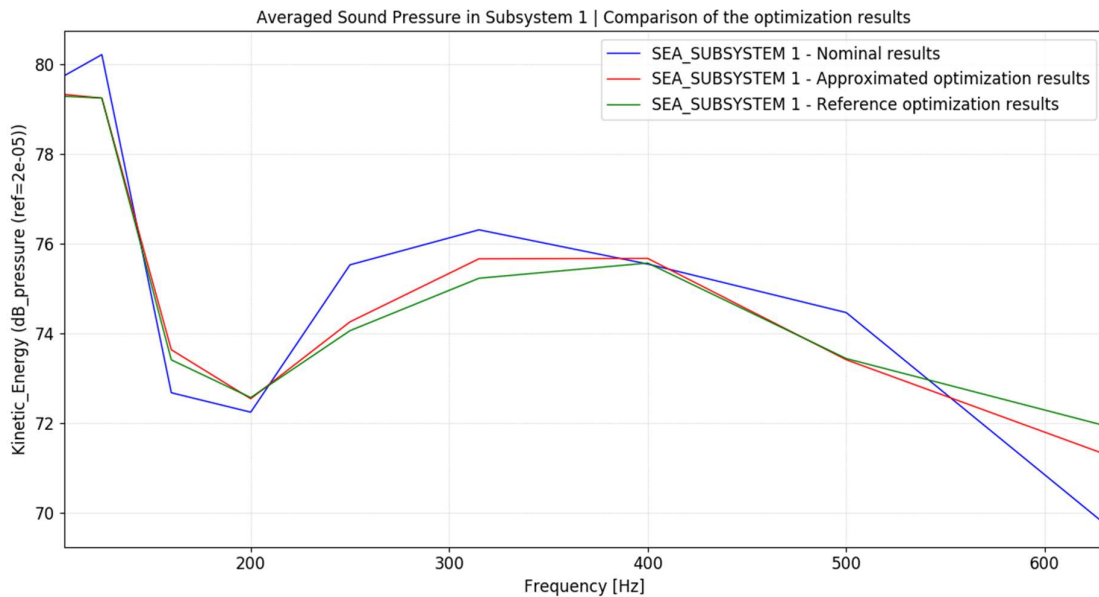
Figure 49. Results comparison of the distinct optimization approaches

6.4.1 Implementation impact on the performance

In the whole process of the virtual SEA analysis, there are different steps of the procedure at which the performance can be measured.

The first comparison that might be done is the evaluation of the PIM, considering that the distribution matrices were already built. Because the expressions derived in this approach are matrices of *n*-modes, they might represent an additional cost to the framework.

In Figure 50, the elapsed time for the evaluation of the PIM procedure has been measured in some iterations of both optimization procedures. It is seen that the cost of the approximation method starts lower and it is increased as more coefficients are considered to the analysis, reaching a limit around 0.055 seconds. When there is no change applied to the model, the average evaluation time is 0.035 seconds. This implies that the method increases this procedure by almost 60%.

However, the magnitude of the time is relatively low compared to the rest of the procedure and this time increase is negligible.
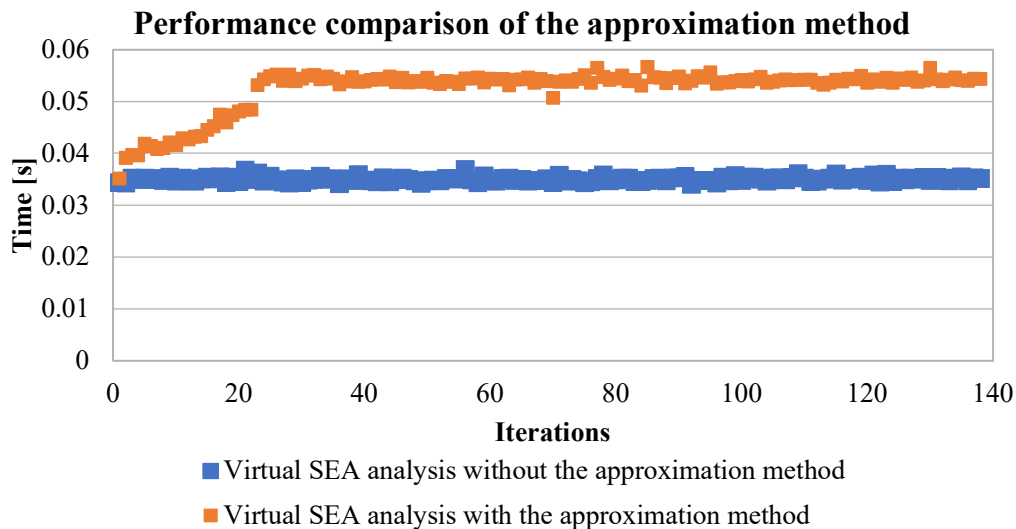
Figure 50. Comparison of the required time to evaluate the PIM

6.4.2 Distribution matrices assembly impact on the performance

To confirm that the performance impact, shown above, will not be a concern to the method implementation, the elapsed time of the virtual SEA framework can be measured. In the case of the optimization with the approximation method, the distribution matrices will be assembled at the start of the analysis or when the modal extraction is performed. However, for the second optimization, the procedure must be done at each iteration.

Thus, it is seen that the build of the distribution matrices will have a much higher impact than the implementation of the approximation method. Figure 51 shows that in this example, the evaluation of the approximation method is around 2 seconds and if the distribution matrices must be assembled, the cost is increased to 7 seconds, around 3.5 times higher.

Therefore, within the whole context of the Virtual SEA, the PIM evaluation cost is negligible and the increase due to the approximation expressions is not a performance concern.

Impact of the distribution matrices build on performance
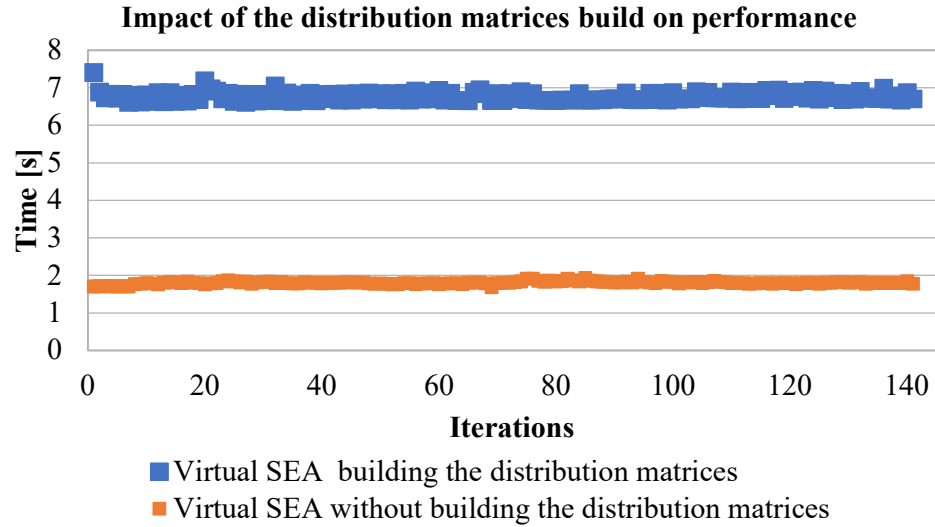
Figure 51. Comparison of the Virtual SEA elapsed time in both approaches

6.4.3 Computational cost of the modal extraction

At last, the computational time of the modal extraction was also measured and shown in Figure 52. It can be concluded that the procedure would be the greatest hindrance if an optimization procedure is desired.

The cost of one modal extraction represents around 75% of the iteration time in the second optimization and it is equivalent to at least 17 iterations of the virtual SEA with the approximation method.
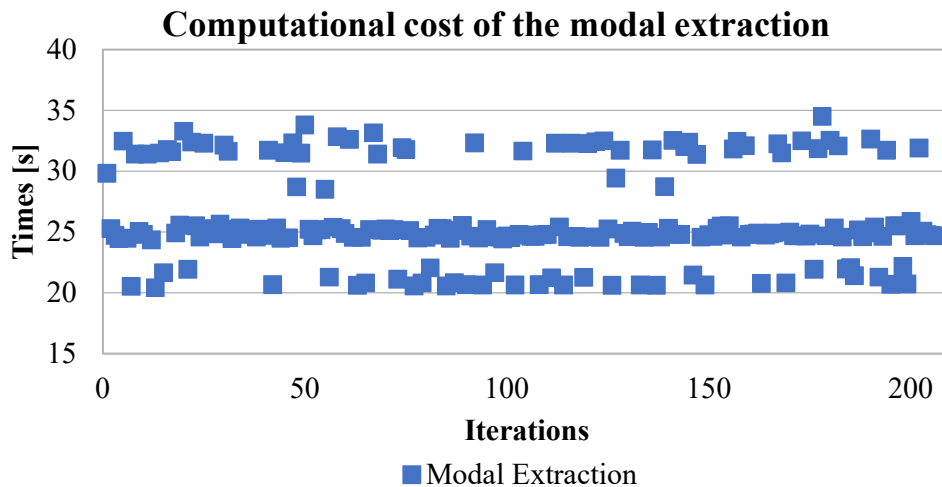
Computational cost of the modal extraction

Figure 52. The computational cost of the modal extraction

7. CONCLUSIONS

Within this study, the application of the Statistical Energy Analysis in a numerical scope could be deeply analyzed, and through derivations of its theoretical expressions, an additional innovative approach could be implemented in its framework. Due to the achieved computational improvements coming from the derived approximation method for perturbated SEA models, an optimization script for the Actran Virtual SEA could be developed and validated with a numerical model.

At first, the Virtual SEA has been performed with a simplified midship cross-section and the intention of the study was to validate the developed method and offer an optimized configuration to it. However, due to the issues related to the presence of excessive local modes in its modal extraction and limitations in the current implementation (which is inherent to Actran and under correction), the application of the method to the model would be unviable.

The objective of the study was to develop a method that allowed the prediction of the energy levels for a SEA model with modified mechanical properties, without the re-extraction of the modal basis and the distribution matrices assembly. Thus, it would be possible to quickly evaluate the energy levels for different configurations of mass, stiffness, and damping on each subsystem.

The first and most straightforward approach was to manipulate the energetic results of the Power Injection Method since they are utilized to compose the SEA matrix. However, the approach could only achieve trivial results that could be understood when analyzing the SEA expressions with more caution. Nevertheless, the implementation of the damping coefficient was successful on its first implementation attempt. The perturbation of the damping related terms before the SEA composition was effective and a global perturbed result was achieved. Thus, the greatest concern became the implementation of the mass and stiffness coefficients.

The following approaches tried to modify parameters related to the PIM with the expectation that the changes would be reflected in the SEA matrix composition. Thus, the modal mass and stiffness of the model were manipulated by weighted averages over the subsystems. These terms are utilized to calculate the frequency integrals that will determine the contribution of the resonant modes to the response of the system.

This approach affected the global energy levels of the model. However, the averaged coefficient could not efficiently represent the magnitudes of change. Thus, it was verified that the changes in the distribution matrices were not negligible and their values should also be

modified by the perturbation coefficients. A similar approach of weighted coefficients only affected slightly the energy results.

It became evident that the changes in the mass and stiffness of the subsystems provided more substantial changes to the model than initially expected. Since the change of these parameters affects the eigenfrequencies of the model, perturbation expressions could be derived from the first-order derivation of the eigenproblem equation.

Once these expressions were efficiently implemented, several tests were performed to validate the approximations. In these verifications, it has been seen that when a subsystem has its mass perturbed, the changes in its stiffness matrix have a greater inaccuracy than expected. Therefore, this ill-conditioned behavior has initially restricted the method to the evaluations of the averaged kinetic energy since it is independent of the stiffness matrices. In addition, the averaged potential energies might be calculated with the approximation method by only changing its stiffness parameters or with the consciousness that if its mass is perturbated, the energy level accuracy will be diminished.

At last, the optimization scripts could be implemented and tested against a conventional approach where the modal extraction and the distribution matrices assemblies are performed at each iteration. Both approaches achieved feasible results that assess the sensitivity of the mass and stiffness of the model with respect to the averaged kinetic energy. However, the optimization procedure based on the approximation method is several times faster than its alternative.

Thus, the innovative developed method in this thesis provides a powerful tool that can be utilized in many unique approaches to solve or improve the NVH behavior of any design. The optimization procedure can be easily modified according to the needs of the designer, and the optimum solution can be achieved at negligible or reasonable additional cost.

8. FURTHER STEPS

As mentioned previously, there are some improvement points in the current approach that must be evaluated but there are also additional extensions that can be developed to aid in the robustness of the software.

8.1 Perform the Optimization of the Ship Model

Due to the issues related to the excessive local modes in the modal extraction, the model could not be utilized for the validation due to the inherent uncertainties associated with it. In addition, the current implementation has a limitation since it can only be applied to a model whose subsystems are composed of a single patch. The latter issue is related to Actran's current framework and it is already being solved. Thus, when the modal basis issues shown in this study are solved, the optimization procedure can be applied to the example.

In addition, the noise sources and the added mass could be assessed more realistically to achieve results that correspond better to practical applications. Besides, all the assessments so far were performed only on the structure in a vacuum, and to retrieve the correct noise levels in the cabins, the acoustic cavities must be added to the model.

8.2 Investigate the Stiffness Distribution Matrix Prediction

The ill-conditioned behavior of the prediction of the stiffness matrix for a subsystem that has its mass perturbed is still unknown. The curious incongruency is that the change applied to the stiffness distribution matrix to all the remaining subsystems represents the change with good accuracy. Therefore, a solution to this source of additional imprecision must be investigated.

8.3 Elaboration of a Research Paper

As the method could be efficiently implemented and all the main goals of the thesis could be achieved, a scientific research paper will be written with the intent to divulge it in a conference or scientific journal, explaining the innovative developed method and the results achieved.

8.4 Extension of the Fluid and Structure Coupling

At the moment, the Virtual SEA solver can tackle light fluid couplings such as air cavities, which are useful to predict the onboard noise of the cabins and even open spaces. Nevertheless, as the underwater radiated noise will be an increasing concern over the next years, the structure coupling available to the Virtual SEA could be extended to handle heavy fluids.

There are studies with interesting approaches where the finite element method has been utilized with the SEA and the radiated underwater noise predicted with the use of the Fast Multipole Boundary Element Method (Blanchet and Caillet, 2012) [14]. However not only the underwater noise is of interest, but other applications must be considered, such as the tank sloshing and the water flow through pipes.

9. THE MASTERSHIP FRAMEWORK

This master thesis has been developed in collaboration with the company Free Field Technologies (FFT) and the implemented methods have been done within the source code of the software Actran.

The frameworks of Actran Energy Analysis and Virtual Statistical Energy Analysis are pre-existing state-of-the-art solutions. Thus, the scope of the thesis was to add functionalities to these solvers, either based on their existing functions or by creating new ones and implement the developed approximated method.

The code implementation of the approximation approaches, changes in the GUI, the optimization scripts and validation attempts were all performed by the author of this thesis with the support of FFT's vibroacoustic team whenever adversities were identified, being these related either to the code implementation or theoretical aspect. To monitor the progress of the project, weekly meetings were made to discuss workarounds and new strategies in case issues were identified. Mostly these meetings were made with the following engineers: Benoit van den Nieuwenhof, Eveline Rossel, Panagiotis Antoniadis, and the author of this thesis. Other eventual meetings took place to share the progress of the thesis and discuss possible issues. These meetings were less frequent but not less important, composed by the previously mentioned engineers with the addition, not necessarily in the same meeting, of the following engineers: Gregory Lielens, Jonathan Jacqmot, Phillipe Rigo, Thomas Lindemann, and Yves Detandt.

10. ACKNOWLEDGMENTS

I would like to dedicate this section to express my gratitude. Firstly to Prof. Dr. Philippe Rigo, Prof. Dr. Patrick Kaeding, Dr. Thomas Lindemann, and all the EMSHIP+ organizers who provided me access to this master program which helped me develop, more than I could ever imagine, personally and professionally. I also want to thank Dr. Yves Detandt who accepted and believed in me to perform this thesis and welcomed me at the FFT.

I am also sincerely grateful to all the FFT staff who were always supportive and friendly, in special, Dr. Benoit van den Nieuwenhof, Dr. Eveline Rossel and Dr. Panagiotis Antoniadis who worked closely to me, sharing their great technical knowledge, providing interesting approaches to achieve the thesis goals and cunning workarounds when difficulties were found. It can be safely said that the outcomes of this study would not be possible without their contributions and guidance.

At last, I would like to thank God, my family, in special my mother, father and sister, friends, and former colleagues who supported and helped me to grow as a better person. Their contribution was essential to the accomplishment of this thesis.

BIBLIOGRAPHY

[1] K. De Langhe, "High Frequency Vibrations: Contributions to experimental and computational SEA parameters identifications techniques," UCL, Leuven, 1996.

[2] Maritime Safety Committee, "Code on Noise Levels on Board Ships," 2012.

[3] B. Southall, A. Scholik-Schlomer, L. Hatch, T. Bergmann, M. Jasny, K. Metcalf, L. Weilgart and A. Wright, " Underwater Noise from Large Commercial Ships—International Collaboration for Noise Reduction," 2017.

[4] R. Seiler, "Structure-borne noise reduction of gearboxes in maritime application," 2019.

[5] B. M. a. P. Shorter, "Energy Flow Models from Finite Element Analysis," *Journal of Sound and Vibration,* no. 233, pp. 369-389, 2000.

[6] S. Neumark, "Concept of Complex Stiffness Applied to Problems of Oscillations with Viscous and Hysteric Damping," H.M. Stationery Office, London, 1962.

[7] K.-J. Bathe, Finite Element Procedures, Watertown: Prentice Hall, Pearson Education, Inc., 2014.

[8] B. Mace, "Statistical energy analysis, energy distribution models and system models and system modes," *Journal of Sound and Vibration,* no. 264, pp. 391-409, 2003.

[9] Free Fields Technologies SA, Actran 20 User's Guide - Volume 1: Installation, Operations, Theory and Utilities, Belgium, 2019.

[10] R. Lyon and R. Maidanik, "Power flow between linearly coupled oscillators.," 1962.

[11] P. Smith, "Response and radiation of structural modes excited by sound," 1962.

[12] Det Norske Veritas, "Part 6 Additional class notations Chapter 8 Living and working conditions," in *Rules for Classification*, Hovik, Norway, 2019.

[13] R. B. Nelson, "Simplified Calculation of Eigenvector Derivatives," *AIAA JOURNAL,* vol. 14, no. 9, pp. 1201-1205, 1976.

[14] Danish Environmental Protection Agency, "Noise from ships in ports: possibilities for noise reduction," 2010.

APPENDIX A – SEA PARAMETERS OF EACH SUBSYSTEM

SEA Parameters od the Subsystem 1

SEA Parameters od the Subsystem 2

SEA Parameters od the Subsystem 3

SEA Parameters od the Subsystem 4

SEA Parameters od the Subsystem 5